FERMILAB-CONF-11-354-E
CDF Note 10606
D0 Note 6226

Combined CDF and D0 Upper Limits on Standard Model Higgs Boson Production with up to 8.6 fb^{-1} of Data

The TEVNPH Working Group*

for the CDF and D0 Collaborations

July 27, 2011

We combine results from CDF and D0 on direct searches for the standard model (SM) Higgs boson (H) in $p\bar{p}$ collisions at the Fermilab Tevatron at $\sqrt{s} = 1.96$ TeV. Compared to the previous Tevatron Higgs boson search combination more data have been added, additional channels have been incorporated, and some previously used channels have been reanalyzed to gain sensitivity. We use the MSTW08 parton distribution functions and the latest theoretical cross sections when comparing our limits to the SM predictions. With up to 8.2 fb^{-1} of data analyzed at CDF and up to 8.6 fb^{-1} at D0, the 95% C.L. our upper limits on Higgs boson production are factors of 1.17, 1.71, and 0.48 times the values of the SM cross section for Higgs bosons of mass m_H =115 GeV/c^2, 140 GeV/c^2, and 165 GeV/c^2, respectively. The corresponding median upper limits expected in the absence of Higgs boson production are 1.16, 1.16, and 0.57. There is a small ($\approx 1\sigma$) excess of data events with respect to the background estimation in searches for the Higgs boson in the mass range $125 < m_H < 155$ GeV/c^2. We exclude, at the 95% C.L., a new and larger region at high mass between $156 < m_H < 177$ GeV/c^2, with an expected exclusion region of $148 < m_H < 180$ GeV/c^2.

Preliminary Results

* The Tevatron New-Phenomena and Higgs Working Group can be contacted at TEVNPHWG@fnal.gov. More information can be found at http://tevnphwg.fnal.gov/.

I. INTRODUCTION

The search for a mechanism for electroweak symmetry breaking, and in particular for a standard model (SM) Higgs boson, has been a major goal of particle physics for many years, and is a central part of the Fermilab Tevatron physics program. Both the CDF and D0 collaborations have performed new combinations [1, 2] of multiple direct searches for the SM Higgs boson. The new searches include more data, additional channels, and improved analysis techniques compared to previous analyses. The sensitivities of these new combinations significantly exceed those of previous combinations [3, 4].

In this note, we combine the most recent results of all such searches in $p\bar{p}$ collisions at $\sqrt{s} = 1.96$ TeV. The analyses combined here seek signals of Higgs bosons produced in association with a vector boson ($q\bar{q} \to W/ZH$), through gluon-gluon fusion ($gg \to H$), and through vector boson fusion (VBF) ($q\bar{q} \to q'\bar{q}'H$) corresponding to integrated luminosities up to 8.2 fb^{-1} at CDF and up to 8.6 fb^{-1} at D0. The Higgs boson decay modes studied are $H \to b\bar{b}$, $H \to W^+W^-$, $H \to ZZ$, $H \to \tau^+\tau^-$ and $H \to \gamma\gamma$.

To simplify the combination, the searches are separated into 165 mutually exclusive final states (71 for CDF and 94 for D0; see Tables II and III) referred to as "analysis sub-channels" in this note. The selection procedures for each analysis are detailed in Refs. [5] through [26], and are briefly described below.

II. ACCEPTANCE, BACKGROUNDS, AND LUMINOSITY

Event selections are similar for the corresponding CDF and D0 analyses, consisting typically of a preselection followed by the use of a multivariate analysis technique with a final discriminating variable to separate signal and background. For the case of $WH \to \ell\nu b\bar{b}$, an isolated lepton (ℓ = electron or muon) and two or three jets required, with one or more b-tagged jets, i.e., identified as containing a weakly-decaying b hadron. Selected events must also display a significant imbalance in transverse momentum (referred to as missing transverse energy or $\not\!\!E_T$). Events with more than one isolated lepton are rejected.

For the D0 $WH \to \ell\nu b\bar{b}$ analyses, the data are split by lepton type and jet multiplicity (two or three jet sub-channels), and whether there are one or two b-tagged jets. As with other D0 analyses targeting the $H \to b\bar{b}$ decay, the $WH \to \ell\nu b\bar{b}$ analyses use a new boosted decision tree based b-tagging algorithm for this combination. The new algorithm is an upgraded version of the neural network b-tagger used previously [27], and includes more information relating to the lifetime of the jet and results in a better discrimination between b and light jets. Unlike previous versions of the analysis the same "loose" b-tagging criterion is applied to both the single (LST) and double (LDT) tag samples, with the output of the b-tagger now being used as an input to the final discriminant. This loose b-tagging criterion corresponds to an identification efficiency of $\approx 80\%$ for true b-jets for a mis-identification rate of $\approx 10\%$. Each sub-channel is analyzed separately. The outputs of boosted decision trees, trained separately for each sample and for each Higgs boson mass, are used as the final discriminating variables in the limit setting procedure. In addition for this combination D0 now uses 8.5 fb^{-1} of data.

For the CDF $WH \to \ell\nu b\bar{b}$ analyses, events are analyzed in two and three jet sub-channels separately, and in each of these samples the events are grouped into various lepton and b-tag categories. Events are broken into separate analysis categories based on the quality of the identified lepton. Separate categories are used for events with a high quality muon or central electron candidate, an isolated track or identified loose muon in the extended muon coverage, a forward electron candidate, and a loose central electron or isolated track candidate. The final two lepton categories, which provide some acceptance for lower quality electrons and single prong tau decays, are used only in the case of two-jet events. Within the lepton categories there are four b-tagging categories considered for two-jet events: two tight b-tags (TDT), one tight b-tag and one loose b-tag (LDT), one tight b-tag and one looser b-tag (LDTX), and a single, tight, b-tag (ST). For three jet events there is no LDTX tagging category and the corresponding events are included within the ST category. In the case of the two jet events, a Bayesian neural network discriminant is trained at each Higgs boson mass within the test range for each of the specific categories (defined by lepton type, b-tagging type, and number of jets), while matrix element (ME) discriminants are used for each three jet event category.

For the $ZH \to \nu\bar{\nu}b\bar{b}$ analyses, the selection is similar to the WH selection, except all events with isolated leptons are rejected and stronger multijet background suppression techniques are applied. Both the CDF and D0 analyses

use a track-based missing transverse momentum calculation as a discriminant against false $\not\!\!E_T$. In addition both CDF and D0 utilize multi-variate techniques, a boosted decision tree at D0 and a neural network at CDF, to further discriminate against the multijet background before b-tagging. There is a sizable fraction of the $WH \to \ell\nu b\bar{b}$ signal in which the lepton is undetected that is selected in the $ZH \to \nu\bar{\nu}b\bar{b}$ samples, so these analyses are also referred to as $VH \to \not\!\!E_T b\bar{b}$. The CDF analysis uses three non-overlapping categories of b-tagged events (TDT, LDT and ST) D0 uses the same loose single (LST) and double tag (LDT) criteria as the $WH \to \ell\nu b\bar{b}$ analyses, with the output of the b-tagger again being used as an input to the final discriminant. CDF uses neural-network outputs for the final discriminating variables, while D0 uses boosted decision tree outputs. For this combination D0 has analysed the 2-jet sample in an exclusive manner, updating both the 1- and 2 b-tag samples to use 8.4 fb^{-1} of data. The exclusive 3-jet sample is currently not included.

The $ZH \to \ell^+\ell^- b\bar{b}$ analyses require two isolated leptons and at least two jets. D0's $ZH \to \ell^+\ell^- b\bar{b}$ analyses separate events into non-overlapping samples of events with either one tight b-tag (TST) or both one tight and one loose b-tags (TLDT). CDF separates events into single tag (ST), double tag (TDT) and loose double tag (LDT) samples. To increase signal acceptance D0 loosens the selection criteria for one of the leptons to include an isolated track not reconstructed in the muon detector ($\mu\mu_{trk}$) or an electron from the inter-cryostat region of the D0 detector (ee_{ICR}). Combined with the dielectron (ee) and dimuon ($\mu\mu$) analyses, these provide four orthogonal analyses, and each uses 8.6 fb^{-1} of data in this combination. CDF uses neural networks to select loose dielectron and dimuon candidates. D0 applies a kinematic fit to optimize reconstruction, while CDF corrects jet energies for $\not\!\!E_T$ using a neural network approach. D0 uses random forests of decision trees to provide the final variables for setting limits. CDF utilizes a multi-layer discriminant based on neural networks where two discriminant functions are used to define three separate regions of the final discriminant function.

For the $H \to W^+W^-$ analyses, signal events are characterized by large $\not\!\!E_T$ and two opposite-signed, isolated leptons. The presence of neutrinos in the final state prevents the accurate reconstruction of the candidate Higgs boson mass. D0 selects events containing electrons and/or muons, dividing the data sample into three final states: e^+e^-, $e^\pm\mu^\mp$, and $\mu^+\mu^-$. Each final state is further subdivided according to the number of jets in the event: 0, 1, or 2 or more ("2+") jets. Each of the three final states each uses 8.1 fb^{-1} of data. Decays involving tau leptons are included in two orthogonal ways. A dedicated analysis ($\mu\tau_{\rm had}$) using 7.3 fb^{-1} of data studying the final state involving a muon and a hadronic tau decay is included in the Tevatron combination. Final states involving other tau decays and mis-identified hadronic tau decays are included in the e^+e^-, $e^\pm\mu^\mp$, and $\mu^+\mu^-$ final state analyses. CDF separates the $H \to W^+W^-$ events in five non-overlapping samples, split into "high s/b" and "low s/b" categories defined by lepton types and the number of reconstructed jets: 0, 1, or 2+ jets. The sample with two or more jets is not split into low s/b and high s/b lepton categories due to the smaller statistics in this channel. A sixth CDF channel is the low dilepton mass ($m_{\ell^+\ell^-}$) channel, which accepts events with $m_{\ell^+\ell^-} < 16$ GeV. A new improvement of the CDF analysis is the ability to recover events with lepton pairs that lie within each other's isolation cones. This improvement leads to a significant increase in sensitivity from the low $m_{\ell^+\ell^-}$ channel, in particular.

The division of events into categories based on the number of reconstructed jets allows the analysis discriminants to separate differing contributions of signal and background processes more effectively. The signal production mechanisms considered are $gg \to H \to W^+W^-$, $WH/ZH \to jjW^+W^-$, and vector-boson fusion. The relative fractions of the contributions from each of the three signal processes and background processes, notably W^+W^- production and $t\bar{t}$ production, are very different in the different jet categories. Dividing our data into these categories provides more statistical discrimination, but introduces the need to evaluate the systematic uncertainties carefully in each jet category. A discussion of these uncertainties is found in Section III.

The D0 e^+e^-, $e^\pm\mu^\mp$, and $\mu^+\mu^-$ final state channels use boosted decision tree outputs as the final discriminants while the $\mu\tau_{\rm had}$ channel uses neural networks. CDF uses neural-network outputs, including likelihoods constructed from calculated matrix-element probabilities as additional inputs for the 0-jet bin.

D0 includes $VH \to \ell^\pm\ell'^\pm + X$ analyses in which the associated vector boson and the W boson from the Higgs boson decay are required to decay leptonically, with like-sign leptons present, thereby defining three like-sign dilepton final states ($e^\pm e^\pm$, $e^\pm\mu^\pm$, and $\mu^\pm\mu^\pm$). The combined output of two decision trees, trained against the instrumental and diboson backgrounds respectively, is used as the final discriminant. CDF also includes a separate analysis of events with same-sign leptons to incorporate additional potential signal from associated production events in which the two leptons (one from the associated vector boson and one from a W boson produced in the Higgs boson decay) have the same charge. CDF additionally incorporates three tri-lepton channels to include additional associated production

contributions in which leptons result from the associated W boson and the two W bosons produced in the Higgs boson decay or where an associated Z boson decays into a dilepton pair and a third lepton is produced in the decay of either of the W bosons resulting from the Higgs boson decay. In the latter case, CDF separates the sample into one jet and two or more jet sub-channels to take advantage of the fact that the Higgs boson candidate mass can be reconstructed from the invariant mass of the two jets, the lepton, and the missing transverse energy.

For the first time CDF includes a search for $H \to ZZ$ using four lepton events. A simple four-lepton invariant mass discriminant is used to separate potential Higgs boson signal events from the non-resonant ZZ background. CDF has also updated its opposite-sign channels in which one of the two lepton candidates is a hadronic tau. Events are separated into e-τ and μ-τ channels. The final discriminants are obtained from boosted decision trees which incorporate both hadronic tau identification and kinematic event variables as inputs. D0 also includes channels in which one of the W bosons in the $H \to W^+W^-$ process decays leptonically and the other decays hadronically. Electron and muon final states are studied separately, each with 5.3 fb^{-1} of data. Random forests are used for the final discriminants.

CDF includes an updated, generic analysis searching for Higgs bosons decaying to tau lepton pairs incorporating contributions from direct $gg \to H$ production, associated WH or ZH production, and vector boson production. CDF also includes for the first time an analysis of events that contain one reconstructed lepton ($\ell = e$ or μ) in addition to a tau lepton pair focusing on associated production where $H \to \tau\tau$ and an additional lepton is produced in the decay of the W or Z boson. For the generic search, events with either one or two jets are separated into two independent analysis channels. The final discriminant for setting limits is obtained using four boosted decision tree discriminants, each designed to discriminate the signal against one of the major backgrounds (QCD multijets, W plus jets, $Z/\gamma^* \to \tau^+\tau^-$, and $Z/\gamma^* \to \ell^+\ell^-$ where $\ell = e$ or μ). In the new analysis events are separated into three tri-lepton categories (e-μ-$\tau_{\rm had}$, ℓ-ℓ-$\tau_{\rm had}$, and ℓ-$\tau_{\rm had}$-$\tau_{\rm had}$). The final discriminants are likelihoods based on Support Vector Machine (SVM) [28] outputs obtained using separate trainings for the signal against each of the primary backgrounds (Z plus jets, $t\bar{t}$, and dibosons). The D0 $\ell^{\pm}\tau^{\mp}_{\rm had}jj$ analysis likewise includes direct $gg \to H$ production, associated WH or ZH production, and vector boson production. Decay of the Higgs boson to both tau and W boson pairs is considered. A final state consisting of one leptonic tau decay, one hadronic hadronic tau decay and two jets is required. Both muonic and electronic sub-channels use 4.3 fb^{-1} The output of boosted decision trees is used as the final discriminant.

CDF incorporates an older all-hadronic analysis, which results in two b-tagging sub-channels (TDT and LDT) for both WH/ZH and VBF production to the $jjb\bar{b}$ final state. Events with either four or five reconstructed jets are selected, and at least two must be b-tagged. The large QCD multijet backgrounds are modeled from the data by applying a measured mistag probability to the non b-tagged jets in events containing a single b-tag. Neural network discriminants based on kinematic event variables including those designed to separate quark and gluon jets are used to obtain the final limits.

D0 and CDF both contribute analyses searching for Higgs bosons decaying into diphoton pairs. The CDF analysis looks for a signal peak in the diphoton invariant mass spectrum above the smooth background originating from standard QCD production. Signal acceptance has been increased in the updated analysis by including forward (plug) calorimeter candidates as well as central photon conversion candidates. Events are now separated into four independent analysis channels based on the photon candidates contained within the event: two central candidates (CC), one central and one plug candidate (CP), one central and one central conversion candidate (CC-Conv), or one plug and one central conversion candidate (PC-Conv). In the D0 analysis the contribution of jets misidentified as photons is reduced by combining information sensitive to differences in the energy deposition from these particles in the tracker, calorimeter and central preshower in a neural network. The output of boosted decision trees, rather than the diphoton invariant mass, is used as the final discriminating variable. The transverse energies of the leading two photons along with the azimuthal opening angle between them and the diphoton invariant mass and transverse momentum are used as input variables. A sizeable improvement in sensitivity ($\approx 30\%$) beyond that achieved with the invariant mass is obtained.

CDF for the first time includes three non-overlapping sets of analysis channels searching for the process $t\bar{t}H \to t\bar{t}b\bar{b}$. One set of channels selects events with a reconstructed lepton, large missing transverse energy, and four or five reconstructed jets. These events are further sub-divided into five b-tagging categories (three tight b-tags (TTT), two tight and one loose b-tags (TTL) , one tight and two loose b-tags (TLL), two tight b-tags (TDT), and one tight and one loose b-tags (LDT)). Ensembles of neural network discriminants trained at each mass point are used to set limits.

A second set of channels selects events with no reconstructed lepton. These events are separated into two categories, one containing events with large missing transverse energy and five to nine reconstructed jets and another containing events with low missing transverse energy and seven to ten reconstructed jets. Events in these two channels are required to have a minimum of two b-tagged jets based on a neural network tagging algorithm. Events with three or more b-tags are analyzed in separate channels from those with exactly two tags. Two stages of neural network discriminants are used (the first to help reject large multijet backgrounds and the second to separate potential $t\bar{t}H$ signal events from $t\bar{t}$ background events).

For both CDF and D0, events from QCD multijet (instrumental) backgrounds are typically measured in independent data samples using several different methods. For CDF, backgrounds from SM processes with electroweak gauge bosons or top quarks were generated using PYTHIA [29], ALPGEN [30], MC@NLO [31], and HERWIG [32] programs. For D0, these backgrounds were generated using PYTHIA, ALPGEN, and COMPHEP [33], with PYTHIA providing parton-showering and hadronization for all the generators. These background processes were normalized using either experimental data or next-to-leading order calculations (including MCFM [34] for the $W+$ heavy flavor process).

III. SIGNAL PREDICTIONS

We normalize our Higgs boson signal predictions to the most recent high-order calculations available. The $gg \to H$ production cross section we use is calculated at next-to-next-to leading order (NNLO) in QCD with a next-to-next-to leading log (NNLL) resummation of soft gluons; the calculation also includes two-loop electroweak effects and handling of the running b quark mass [35, 36]. The numerical values in Table I are updates [37] of these predictions with m_t set to 173.1 GeV/c^2 [38], and with a treatment of the massive top and bottom loop corrections up to next-to-leading-order (NLO) + next-to-leading-log (NLL) accuracy. The factorization and renormalization scale choice for this calculation is $\mu_F = \mu_R = m_H$. These calculations are refinements of the earlier NNLO calculations of the $gg \to H$ production cross section [39–41]. Electroweak corrections were computed in Refs. [42, 43]. Soft gluon resummation was introduced in the prediction of the $gg \to H$ production cross section in Ref. [44]. The $gg \to H$ production cross section depends strongly on the gluon parton density function, and the accompanying value of $\alpha_s(q^2)$. The cross sections used here are calculated with the MSTW 2008 NNLO PDF set [45], as recommended by the PDF4LHC working group [46]. The inclusive Higgs boson production cross sections are listed in Table I.

For analyses that consider inclusive $gg \to H$ production but do not split it into separate channels based on the number of reconstructed jets, we use the inclusive uncertainties from the simultaneous variation of the factorization and renormalization scale up and down by a factor of two. We use the prescription of the PDF4LHC working group for evaluating PDF uncertainties on the inclusive production cross section. QCD scale uncertainties that affect the cross section via their impacts on the PDFs are included as a correlated part of the total scale uncertainty. The remainder of the PDF uncertainty is treated as uncorrelated with the QCD scale uncertainty.

For analyses seeking $gg \to H$ production that divide events into categories based on the number of reconstructed jets, we employ a new approach for evaluating the impacts of the scale uncertainties. Following the recommendations of Ref. [47], we treat the QCD scale uncertainties obtained from the NNLL inclusive [35, 36], NLO one or more jets [48], and NLO two or more jets [49] cross section calculations as uncorrelated with one another. We then obtain QCD scale uncertainties for the exclusive $gg \to H + 0$ jet, 1 jet, and 2 or more jet categories by propagating the uncertainties on the inclusive cross section predictions through the subtractions needed to predict the exclusive rates. For example, the H+0 jet cross section is obtained by subtracting the NLO $H + 1$ or more jet cross section from the inclusive NNLL+NNLO cross section. We now assign three separate, uncorrelated scale uncertainties which lead to correlated and anticorrelated uncertainty contributions between exclusive jet categories. The procedure in Ref. [48] is used to determine PDF model uncertainties. These are obtained separately for each jet bin and treated as 100% correlated between jet bins and between D0 and CDF.

The scale choice affects the p_T spectrum of the Higgs boson when produced in gluon-gluon fusion, and this effect changes the acceptance of the selection requirements and also the shapes of the distributions of the final discriminants. The effect of the acceptance change is included in the calculations of Ref. [48] and Ref. [49], as the experimental requirements are simulated in these calculations. The effects on the final discriminant shapes are obtained by reweighting the p_T spectrum of the Higgs boson production in our Monte Carlo simulation to higher-order calculations. The Monte Carlo signal simulation used by CDF and D0 is provided by the LO generator PYTHIA [29] which includes a parton

shower and fragmentation and hadronization models. We reweight the Higgs boson p_T spectra in our PYTHIA Monte Carlo samples to that predicted by HQT [50] when making predictions of differential distributions of $gg \to H$ signal events. To evaluate the impact of the scale uncertainty on our differential spectra, we use the RESBOS [51] generator, and apply the scale-dependent differences in the Higgs boson p_T spectrum to the HQT prediction, and propagate these to our final discriminants as a systematic uncertainty on the shape, which is included in the calculation of the limits.

We include all significant Higgs boson production modes in the high-mass search. Besides gluon-gluon fusion through virtual quark loops (ggH), we include Higgs boson production in association with a W or Z vector boson (VH), and vector boson fusion (VBF). For the low-mass searches, we target the WH, ZH, VBF, and $t\bar{t}H$ production modes with specific searches, including also those signal components not specifically targeted but which fall in the acceptance nonetheless. Our WH and ZH cross sections are from Ref. [52]. This calculation starts with the NLO calculation of V2HV [53] and includes NNLO QCD contributions [54], as well as one-loop electroweak corrections [55]. We use the VBF cross section computed at NNLO in QCD in Ref. [56]. Electroweak corrections to the VBF production cross section are computed with the HAWK program [57], and are small and negative (2-3%) in the Higgs boson mass range considered here. We include these corrections in the VBF cross sections used for this result. The $t\bar{t}H$ production cross sections we use are from Ref. [58].

In order to predict the kinematic distributions of Higgs boson signal events, CDF and D0 use the PYTHIA [29] Monte Carlo program, with CTEQ5L and CTEQ6L1 [59] leading-order (LO) parton distribution functions.

The Higgs boson decay branching ratio predictions used for this result are those of Ref. [60]. In this calculation, the partial decay widths for all Higgs boson decays except to pairs of W and Z bosons are computed with HDECAY [61], and the W and Z pair decay widths are computed with PROPHECY4F [62]. The relevant decay branching ratios are listed in Table I. The uncertainties on the predicted branching ratios from uncertainties in m_b, m_c, and α_s are presented in Ref. [63].

Tables II and III summarize, for CDF and D0 respectively, the integrated luminosities, the Higgs boson mass ranges over which the searches are performed, and references to further details for each analysis.

IV. DISTRIBUTIONS OF CANDIDATES

All analyses provide binned histograms of the final discriminant variables for the signal and background predictions, itemized separately for each source, and the observed data. The number of channels combined is large, and the number of bins in each channel is large. Therefore, the task of assembling histograms and checking whether the expected and observed limits are consistent with the input predictions and observed data is difficult. We therefore provide histograms that aggregate all channels' signal, background, and data together. In order to preserve most of the sensitivity gain that is achieved by the analyses by binning the data instead of collecting them all together and counting, we aggregate the data and predictions in narrow bins of signal-to-background ratio, s/b. Data with similar s/b may be added together with no loss in sensitivity, assuming similar systematic errors on the predictions. The aggregate histograms do not show the effects of systematic uncertainties, but instead compare the data with the central predictions supplied by each analysis.

The range of s/b is quite large in each analysis, and so $\log_{10}(s/b)$ is chosen as the plotting variable. Plots of the distributions of $\log_{10}(s/b)$ are shown for Higgs boson masses of 115, 140, and 165 GeV/c^2 in Figure 1. These distributions can be integrated from the high-s/b side downwards, showing the sums of signal, background, and data for the most pure portions of the selection of all channels added together. These integrals can be seen in Figure 2. The most significant candidates are found in the bins with the highest s/b; an excess in these bins relative to the background prediction drives the Higgs boson cross section limit upwards, while a deficit drives it downwards. The lower-s/b bins show that the modeling of the rates and kinematic distributions of the backgrounds is very good. The integrated plots show a slight excess of events in the highest-s/b bins for the analyses seeking a Higgs boson mass of 115 GeV/c^2 and 140 GeV/c^2, and a slight deficit of events in the highest-s/b bins for the analyses seeking a Higgs boson of mass 165 GeV/c^2.

We also show the distributions of the data after subtracting the expected background, and compare that with the expected signal yield for a Standard Model Higgs boson, after collecting all bins in all channels sorted by s/b. These

TABLE I: The production cross sections and decay branching fractions for the SM Higgs boson assumed for the combination.

m_H (GeV/c^2)	$\sigma_{gg\to H}$ (fb)	σ_{WH} (fb)	σ_{ZH} (fb)	σ_{VBF} (fb)	$\sigma_{t\bar{t}H}$ (fb)	$B(H\to b\bar{b})$ (%)	$B(H\to c\bar{c})$ (%)	$B(H\to\tau^+\tau^-)$ (%)	$B(H\to W^+W^-)$ (%)	$B(H\to ZZ)$ (%)	$B(H\to\gamma\gamma)$ (%)
100	1821.8	291.90	169.8	97.2	8.000	79.1	3.68	8.36	1.11	0.113	0.159
105	1584.7	248.40	145.9	89.7	7.062	77.3	3.59	8.25	2.43	0.215	0.178
110	1385.0	212.00	125.7	82.7	6.233	74.5	3.46	8.03	4.82	0.439	0.197
115	1215.9	174.50	103.9	76.4	5.502	70.5	3.27	7.65	8.67	0.873	0.213
120	1072.3	150.10	90.2	70.7	4.857	64.9	3.01	7.11	14.3	1.60	0.225
125	949.3	129.50	78.5	65.3	4.279	57.8	2.68	6.37	21.6	2.67	0.230
130	842.9	112.00	68.5	60.4	3.769	49.4	2.29	5.49	30.5	4.02	0.226
135	750.8	97.20	60.0	55.9	3.320	40.4	1.87	4.52	40.3	5.51	0.214
140	670.6	84.60	52.7	51.8	2.925	31.4	1.46	3.54	50.4	6.92	0.194
145	600.6	73.70	46.3	48.1	2.593	23.1	1.07	2.62	60.3	7.96	0.168
150	539.1	64.40	40.8	44.6	2.298	15.7	0.725	1.79	69.9	8.28	0.137
155	484.0	56.20	35.9	41.2	2.037	9.18	0.425	1.06	79.6	7.36	0.100
160	432.3	48.50	31.4	38.2	1.806	3.44	0.159	0.397	90.9	4.16	0.0533
165	383.7	43.60	28.4	36.0	1.607	1.19	0.0549	0.138	96.0	2.22	0.0230
170	344.0	38.50	25.3	33.4	1.430	0.787	0.0364	0.0920	96.5	2.36	0.0158
175	309.7	34.00	22.5	31.0	1.272	0.612	0.0283	0.0719	95.8	3.23	0.0123
180	279.2	30.10	20.0	28.8	1.132	0.497	0.0230	0.0587	93.2	6.02	0.0102
185	252.1	26.90	17.9	26.9	1.004	0.385	0.0178	0.0457	84.4	15.0	0.00809
190	228.0	24.00	16.1	25.0	0.890	0.315	0.0146	0.0376	78.6	20.9	0.00674
195	207.2	21.40	14.4	23.3	0.789	0.270	0.0125	0.0324	75.7	23.9	0.00589
200	189.1	19.10	13.0	21.6	0.700	0.238	0.0110	0.0287	74.1	25.6	0.00526

TABLE II: Luminosity, explored mass range and references for the different processes and final states ($\ell = e$ or μ) for the CDF analyses. The generic labels "2×" and "4×" refer to separations based on lepton categories.

Channel	Luminosity (fb^{-1})	m_H range (GeV/c^2)	Reference
$WH \to \ell\nu b\bar{b}$ 2-jet channels 4×(TDT,LDT,ST,LDTX)	7.5	100-150	[5]
$WH \to \ell\nu b\bar{b}$ 3-jet channels 2×(TDT,LDT,ST)	5.6	100-150	[6]
$ZH \to \nu\bar{\nu}b\bar{b}$ (TDT,LDT,ST)	7.8	100-150	[7]
$ZH \to \ell^+\ell^- b\bar{b}$ 2×(TDT,LDT,ST)	7.7	100-150	[8, 9]
$H \to W^+W^-$ 2×(0 jets,1 jet)+(2 or more jets)+(low-$m_{\ell\ell}$)+(e-τ_{had})+(μ-τ_{had})	8.2	110-200	[10]
$WH \to WW^+W^-$ (same-sign leptons)+(tri-leptons)	8.2	110-200	[10]
$ZH \to ZW^+W^-$ (tri-leptons with 1 jet)+(tri-leptons with 2 or more jets)	8.2	110-200	[10]
	8.2	110-200	[11]
$H + X \to \tau^+\tau^-$ (1 jet)+(2 jets)	6.0	100-150	[12]
$WH \to \ell\nu\tau^+\tau^-/ZH \to \ell^+\ell^-\tau^+\tau^-$ (ℓ-ℓ-τ_{had})+(e-μ-τ_{had})+(ℓ-τ_{had}-τ_{had})	6.2	110-150	[13]
$WH + ZH \to jjb\bar{b}$ (GF,VBF)×(TDT,LDT)	4.0	100-150	[14]
$H \to \gamma\gamma$ (CC,CP,CC-Conv,PC-Conv)	7.0	100-150	[15]
$t\bar{t}H \to WWb\bar{b}b\bar{b}$ (lepton) (4jet,5jet)×(TTT,TTL,TLL,TDT,LDT)	6.3	100-150	[16]
$t\bar{t}H \to WWb\bar{b}b\bar{b}$ (no lepton) (low met,high met)×(2 tags,3 or more tags)	5.7	100-150	[17]

TABLE III: Luminosity, explored mass range and references for the different processes and final states ($\ell = e, \mu$) for the D0 analyses.

Channel	Luminosity (fb^{-1})	m_H range (GeV/c^2)	Reference
$WH \to \ell\nu b\bar{b}$ (LST,LDT,2,3 jet)	8.5	100-150	[18]
$ZH \to \nu\bar{\nu}b\bar{b}$ (LST,LDT)	8.4	100-150	[19]
$ZH \to \ell^+\ell^- b\bar{b}$ (TST,TLDT,ee,$\mu\mu$,ee_{ICR},$\mu\mu_{trk}$)	8.6	100-150	[20]
$H+X \to \ell^\pm\tau^\mp_{\text{had}}jj$	4.3	105-200	[21]
$VH \to \ell^\pm\ell^\pm + X$	5.3	115-200	[22]
$H \to W^+W^- \to \ell^\pm\nu\ell^\mp\nu$ (0,1,2+ jet)	8.1	115-200	[23]
$H \to W^+W^- \to \mu\nu\tau_{\text{had}}\nu$	7.3	115-200	[24]
$H \to W^+W^- \to \ell\bar{\nu}jj$	5.4	130-200	[25]
$H \to \gamma\gamma$	8.2	100-150	[26]

background-subtracted distributions are shown in Figure 3 for Higgs boson masses of 115, 140, and 165 GeV/c^2. These graphs also show the remaining uncertainty on the background prediction after fitting the background model to the data within the systematic uncertainties on the rates and shapes in each contributing channel.

V. COMBINING CHANNELS

To gain confidence that the final result does not depend on the details of the statistical formulation, we perform two types of combinations, using Bayesian and Modified Frequentist approaches, which yield limits on the Higgs boson production rate that agree within 10% at each value of m_H, and within 1% on average. Both methods rely on distributions in the final discriminants, and not just on their single integrated values. Systematic uncertainties enter on the predicted number of signal and background events as well as on the distribution of the discriminants in each analysis ("shape uncertainties"). Both methods use likelihood calculations based on Poisson probabilities.

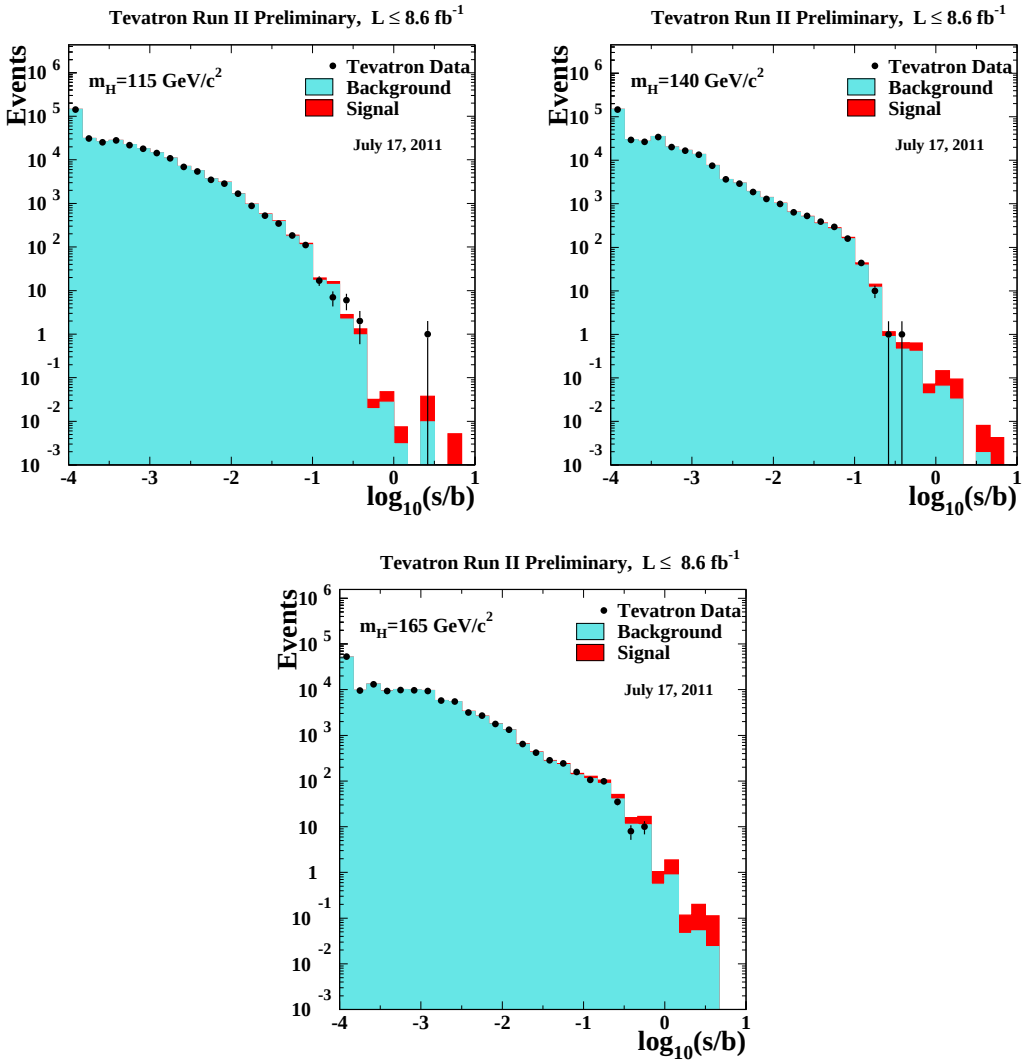

FIG. 1: Distributions of $\log_{10}(s/b)$, for the data from all contributing channels from CDF and D0, for Higgs boson masses of 115, 140, and 165 GeV/c^2. The data are shown with points, and the expected signal is shown stacked on top of the backgrounds. Underflows and overflows are collected into the leftmost and rightmost bins.

A. Bayesian Method

Because there is no experimental information on the production cross section for the Higgs boson, in the Bayesian technique [1] we assign a flat prior for the total number of selected Higgs boson events. For a given Higgs boson mass, the combined likelihood is a product of likelihoods for the individual channels, each of which is a product over histogram bins:

$$\mathcal{L}(R,\vec{s},\vec{b}|\vec{n},\vec{\theta})\times\pi(\vec{\theta}) = \prod_{i=1}^{N_C}\prod_{j=1}^{N_b}\mu_{ij}^{n_{ij}}e^{-\mu_{ij}}/n_{ij}!\times\prod_{k=1}^{n_{np}}e^{-\theta_k^2/2} \quad (1)$$

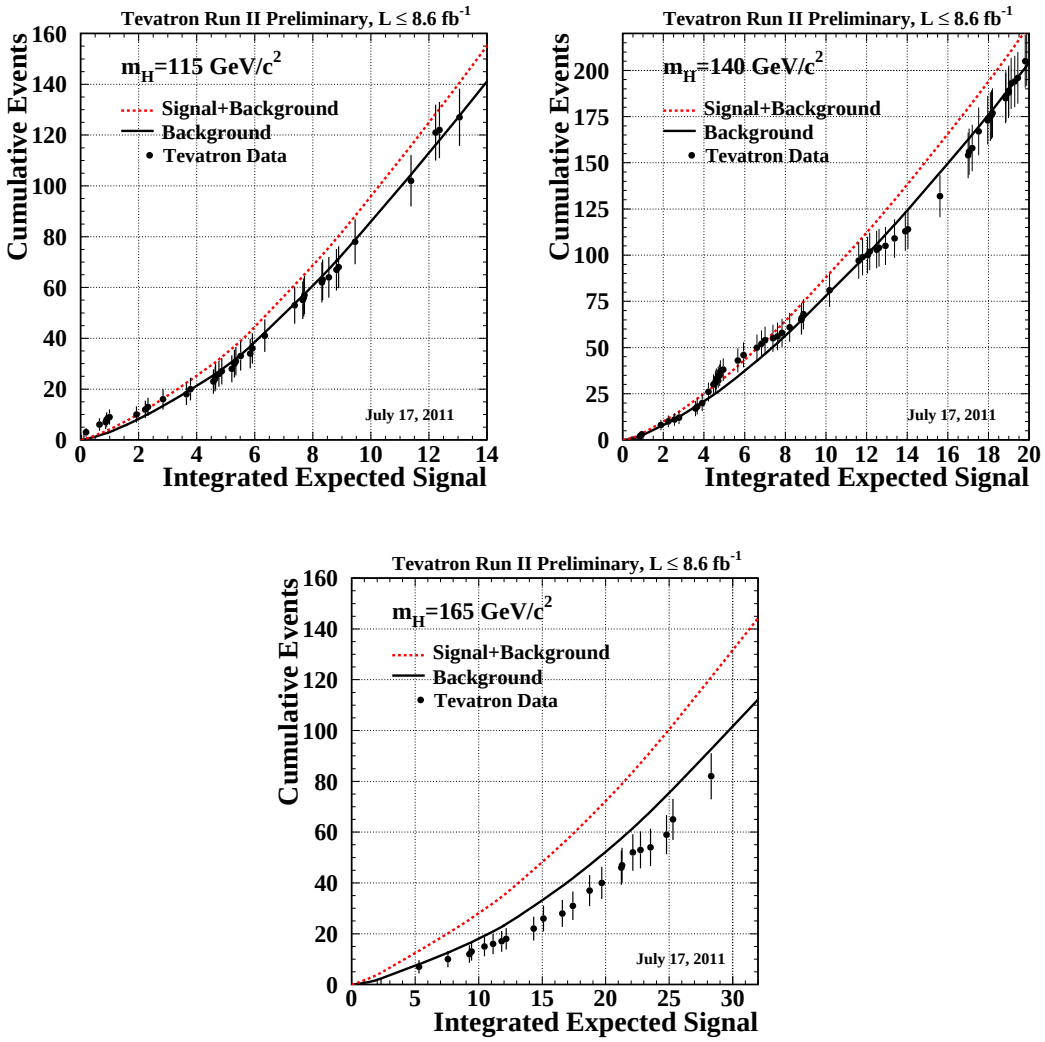

FIG. 2: Integrated distributions of s/b, starting at the high s/b side, for Higgs boson masses of 115, 140, and 165 GeV/c^2. The total signal+background and background-only integrals are shown separately, along with the data sums. Data are only shown for bins that have data events in them.

where the first product is over the number of channels (N_C), and the second product is over N_b histogram bins containing n_{ij} events, binned in ranges of the final discriminants used for individual analyses, such as the dijet mass, neural-network outputs, or matrix-element likelihoods. The parameters that contribute to the expected bin contents are $\mu_{ij} = R \times s_{ij}(\vec{\theta}) + b_{ij}(\vec{\theta})$ for the channel i and the histogram bin j, where s_{ij} and b_{ij} represent the expected background and signal in the bin, and R is a scaling factor applied to the signal to test the sensitivity level of the experiment. Truncated Gaussian priors are used for each of the nuisance parameters θ_k, which define the sensitivity of the predicted signal and background estimates to systematic uncertainties. These can take the form of uncertainties on overall rates, as well as the shapes of the distributions used for combination. These systematic uncertainties can be far larger than the expected SM Higgs boson signal, and are therefore important in the calculation of limits. The truncation is applied so that no prediction of any signal or background in any bin is negative. The posterior density

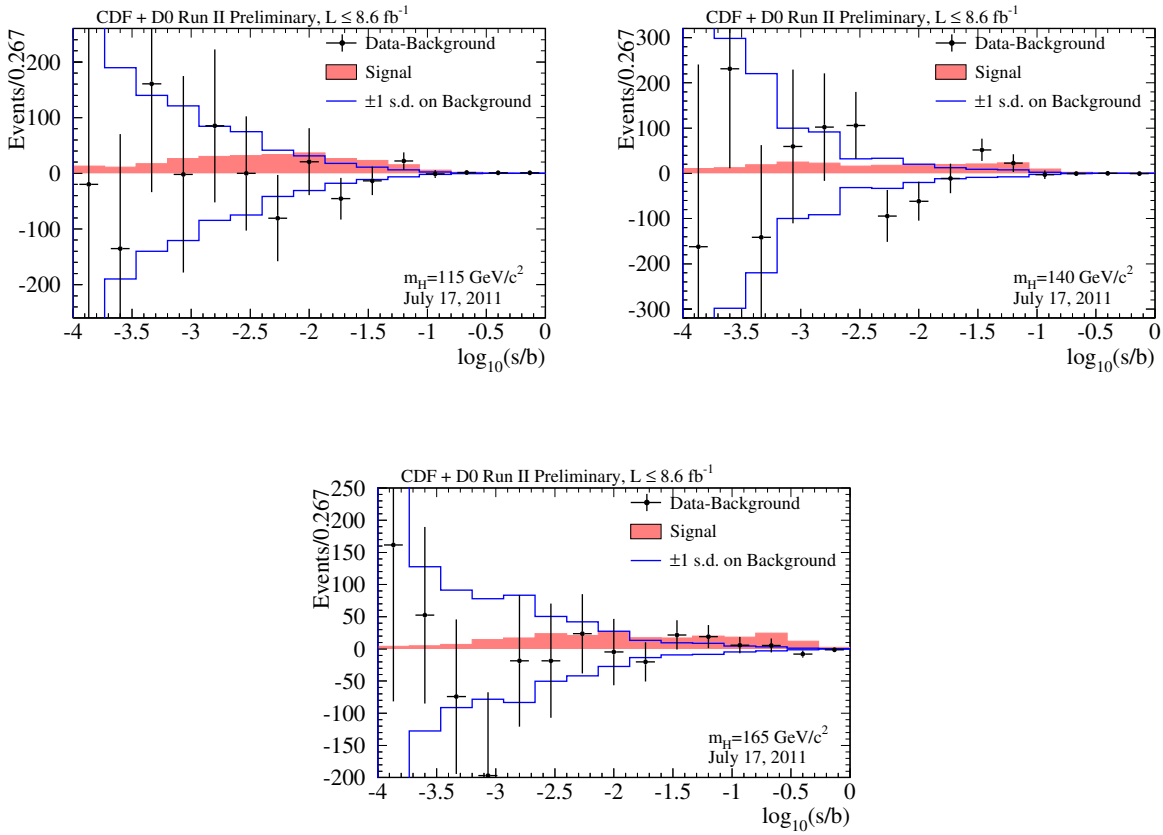

FIG. 3: Background-subtracted data distributions for all channels, summed in bins of s/b, for Higgs boson masses of 115, 140, and 165 GeV/c^2. The background has been fit, within its systematic uncertainties, to the data. The points with error bars indicate the background-subtracted data; the sizes of the error bars are the square roots of the predicted background in each bin. The unshaded (blue-outline) histogram shows the systematic uncertainty on the best-fit background model, and the shaded histogram shows the expected signal for a Standard Model Higgs boson.

function is then integrated over all parameters (including correlations) except for R, and a 95% credibility level upper limit on R is estimated by calculating the value of R that corresponds to 95% of the area of the resulting distribution.

B. Modified Frequentist Method

The Modified Frequentist technique relies on the CL_s method, using a log-likelihood ratio (LLR) as test statistic [2]:

$$LLR = -2\ln\frac{p(\text{data}|H_1)}{p(\text{data}|H_0)}, \tag{2}$$

where H_1 denotes the test hypothesis, which admits the presence of SM backgrounds and a Higgs boson signal, while H_0 is the null hypothesis, for only SM backgrounds and 'data' is either an ensemble of pseudo-experiment data constructed from the expected signal and backgrounds, or the actual observed data. The probabilities p are computed using the best-fit values of the nuisance parameters for each pseudo-experiment, separately for each of the

two hypotheses, and include the Poisson probabilities of observing the data multiplied by Gaussian priors for the values of the nuisance parameters. This technique extends the LEP procedure [64] which does not involve a fit, in order to yield better sensitivity when expected signals are small and systematic uncertainties on backgrounds are large [65].

The CL_s technique involves computing two p-values, CL_{s+b} and CL_b. The latter is defined by

$$1 - CL_b = p(LLR \leq LLR_{obs}|H_0), \tag{3}$$

where LLR_{obs} is the value of the test statistic computed for the data. $1 - CL_b$ is the probability of observing a signal-plus-background-like outcome without the presence of signal, i.e. the probability that an upward fluctuation of the background provides a signal-plus-background-like response as observed in data. The other p-value is defined by

$$CL_{s+b} = p(LLR \geq LLR_{obs}|H_1), \tag{4}$$

and this corresponds to the probability of a downward fluctuation of the sum of signal and background in the data. A small value of CL_{s+b} reflects inconsistency with H_1. It is also possible to have a downward fluctuation in data even in the absence of any signal, and a small value of CL_{s+b} is possible even if the expected signal is so small that it cannot be tested with the experiment. To minimize the possibility of excluding a signal to which there is insufficient sensitivity (an outcome expected 5% of the time at the 95% C.L., for full coverage), we use the quantity $CL_s = CL_{s+b}/CL_b$. If $CL_s < 0.05$ for a particular choice of H_1, that hypothesis is deemed to be excluded at the 95% C.L. In an analogous way, the expected CL_b, CL_{s+b} and CL_s values are computed from the median of the LLR distribution for the background-only hypothesis.

Systematic uncertainties are included by fluctuating the predictions for signal and background rates in each bin of each histogram in a correlated way when generating the pseudo-experiments used to compute CL_{s+b} and CL_b.

C. Systematic Uncertainties

Systematic uncertainties differ between experiments and analyses, and they affect the rates and shapes of the predicted signal and background in correlated ways. The combined results incorporate the sensitivity of predictions to values of nuisance parameters, and include correlations between rates and shapes, between signals and backgrounds, and between channels within experiments and between experiments. More on these issues can be found in the individual analysis notes [5] through [26]. Here we consider only the largest contributions and correlations between and within the two experiments.

1. Correlated Systematics between CDF and D0

The uncertainties on the measurements of the integrated luminosities are 6% (CDF) and 6.1% (D0). Of these values, 4% arises from the uncertainty on the inelastic $p\bar{p}$ scattering cross section, which is correlated between CDF and D0. CDF and D0 also share the assumed values and uncertainties on the production cross sections for top-quark processes ($t\bar{t}$ and single top) and for electroweak processes (WW, WZ, and ZZ). In order to provide a consistent combination, the values of these cross sections assumed in each analysis are brought into agreement. We use $\sigma_{t\bar{t}} = 7.04^{+0.24}_{-0.36}$ (scale) $\pm$ 0.14(PDF) $\pm$ 0.30(mass), following the calculation of Moch and Uwer [66], assuming a top quark mass $m_t = 173.0 \pm 1.2$ GeV/c^2 [38], and using the MSTW2008nnlo PDF set [45]. Other calculations of $\sigma_{t\bar{t}}$ are similar [67].

For single top, we use the NLL t-channel calculation of Kidonakis [68], which has been updated using the MSTW2008nnlo PDF set [45] [69]. For the s-channel process we use [70], again based on the MSTW2008nnlo PDF set. Both of the cross section values below are the sum of the single t and single $\bar{t}$ cross sections, and both assume $m_t = 173 \pm 1.2$ GeV.

$$\sigma_{t-\mathrm{chan}} = 2.10 \pm 0.027(\mathrm{scale}) \pm 0.18(\mathrm{PDF}) \pm 0.045(\mathrm{mass})\mathrm{pb}. \tag{5}$$

$$\sigma_{s-\mathrm{chan}} = 1.05 \pm 0.01(\mathrm{scale}) \pm 0.06\ (\mathrm{PDF}) \pm 0.03\ (\mathrm{mass})\ \mathrm{pb}. \quad (6)$$

Other calculations of $\sigma_{\mathrm{SingleTop}}$ are similar for our purposes [71].

MCFM [34] has been used to compute the NLO cross sections for WW, WZ, and ZZ production [72]. Using a scale choice $\mu_0 = M_V^2 + p_T^2(V)$ and the MSTW2008 PDF set [45], the cross section for inclusive W^+W^- production is

$$\sigma_{W^+W^-} = 11.34^{+0.56}_{-0.49}\ (\mathrm{scale})\ ^{+0.35}_{-0.28}(\mathrm{PDF})\mathrm{pb} \quad (7)$$

and the cross section for inclusive $W^\pm Z$ production is

$$\sigma_{W^\pm Z} = 3.22^{+0.20}_{-0.17}\ (\mathrm{scale})\ ^{+0.11}_{-0.08}\ (\mathrm{PDF})\ \mathrm{pb} \quad (8)$$

For the Z, leptonic decays are used in the definition, with both γ and Z exchange. The cross section quoted above involves the requirement $75 \leq m_{\ell^+\ell^-} \leq 105$ GeV for the leptons from the neutral current exchange. The same dilepton invariant mass requirement is applied to both sets of leptons in determining the ZZ cross section which is

$$\sigma_{ZZ} = 1.20^{+0.05}_{-0.04}\ (\mathrm{scale})\ ^{+0.04}_{-0.03}\ (\mathrm{PDF})\ \mathrm{pb} \quad (9)$$

For the diboson cross section calculations, $|\eta_\ell| < 5$ for all calculations. Loosening this requirement to include all leptons leads to $\sim$+0.4% change in the predictions. Lowering the factorization and renormalization scales by a factor of two increases the cross section, and raising the scales by a factor of two decreases the cross section. The PDF uncertainty has the same fractional impact on the predicted cross section independent of the scale choice. All PDF uncertainties are computed as the quadrature sum of the twenty 68% C.L. eigenvectors provided with MSTW2008 (MSTW2008nlo68cl).

In many analyses, the dominant background yields are calibrated with data control samples. Since the methods of measuring the multijet ("QCD") backgrounds differ between CDF and D0, and even between analyses within the collaborations, there is no correlation assumed between these rates. Similarly, the large uncertainties on the background rates for W+heavy flavor (HF) and Z+heavy flavor are considered at this time to be uncorrelated. The calibrations of fake leptons, unvetoed $\gamma \to e^+e^-$ conversions, b-tag efficiencies and mistag rates are performed by each collaboration using independent data samples and methods, and are therefore also treated as uncorrelated.

2. Correlated Systematic Uncertainties for CDF

The dominant systematic uncertainties for the CDF analyses are shown in the Appendix in Tables VIII and IX for the $WH \to \ell\nu b\bar{b}$ channels, in Table XII for the $WH, ZH \to \not\!\!E_T b\bar{b}$ channels, in Tables XIV and XV for the $ZH \to \ell^+\ell^- b\bar{b}$ channels, in Tables XVII, XVIII, and XIX for the $H \to W^+W^- \to \ell'^\pm\nu\ell'^\mp\nu$ channels, in Table XX for the $WH \to WWW \to \ell'^\pm\ell'^\pm$ and $WH \to WWW \to \ell^\pm\ell'^\pm\ell''^\mp$ channels, in Table XXI for the $ZH \to ZWW \to \ell^\pm\ell^\mp\ell'^\pm$ channels, In Table XXVI for the $H \to 4\ell$ channel, in Tables XXVII, XXVIII, and XXIX for the $t\bar{t}H \to W^+bW^-\bar{b}b\bar{b}$ channels, in Table XXX for the $H \to \tau^+\tau^-$ channels, in Table XXXI for the $WH \to \ell\nu\tau^+\tau^-$ and $ZH \to \ell^+\ell^-\tau^+\tau^-$ channels, in Table XXXII for the WH/ZH and VBF $\to jjb\bar{b}$ channels, and in Table XXXIII for the $H \to \gamma\gamma$ channel. Each source induces a correlated uncertainty across all CDF channels' signal and background contributions which are sensitive to that source. For $H \to b\bar{b}$, the largest uncertainties on signal arise from measured b-tagging efficiencies, jet energy scale, and other Monte Carlo modeling. Shape dependencies of templates on jet energy scale, b-tagging, and gluon radiation ("ISR" and "FSR") are taken into account for some analyses (see tables). For $H \to W^+W^-$, the largest uncertainties on signal acceptance originate from Monte Carlo modeling. Uncertainties on background event rates vary significantly for the different processes. The backgrounds with the largest systematic uncertainties are in general quite small. Such uncertainties are constrained by fits to the nuisance parameters, and they do not affect the result significantly. Because the largest background contributions are measured using data, these uncertainties are treated as uncorrelated for the $H \to b\bar{b}$ channels. The differences in the resulting limits when treating the remaining uncertainties as either correlated or uncorrelated is less than 5%.

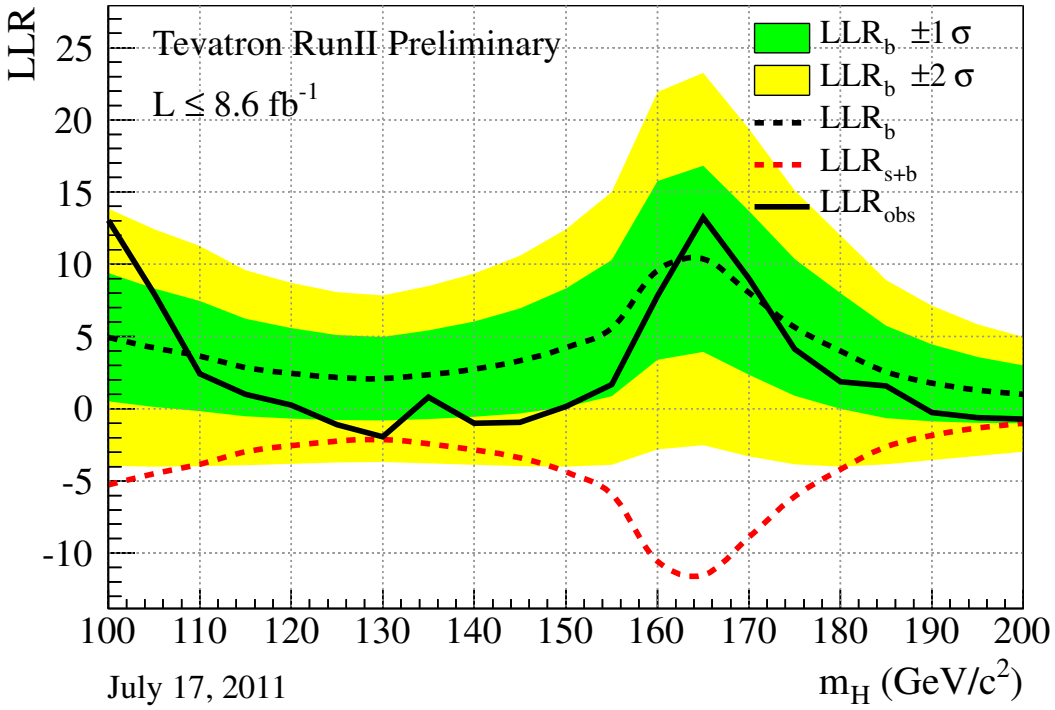

FIG. 4: Distributions of the log-likelihood ratio (LLR) as a function of Higgs boson mass obtained with the CL_s method for the combination of all CDF and D0 analyses. The green and yellow bands correspond to the regions enclosing 1-σ and 2-σ fluctuations of the background, respectively.

3. Correlated Systematic Uncertainties for D0

The dominant systematic uncertainties for the D0 analyses are shown in the Appendix, in Tables X, XI, XIII, XVI, XXII, XXIII, XXIV, XXV, and XXXIV. Each source induces a correlated uncertainty across all D0 channels sensitive to that source. Wherever appropriate the impact of systematic effects on both the rate and shape of the predicted signal and background is included. For the low mass, $H \to b\bar{b}$ analyses, significant sources of uncertainty include the measured b-tagging rate and the normalization of the W and Z plus heavy flavor backgrounds. For the $H \to W^+W^-$and $VH \to \ell^{\pm}\ell'^{\pm} + X$ analyses, significant sources of uncertainty are the measured efficiencies for selecting leptons. For analyses involving jets the determination of the jet energy scale, jet resolution and the multijet background contribution are significant sources of uncertainty. Significant sources for all analyses are the uncertainties on the luminosity and the cross sections for the simulated backgrounds. All systematic uncertainties arising from the same source are taken to be correlated among the different backgrounds and between signal and background.

VI. COMBINED RESULTS

Before extracting the combined limits we study the distributions of the log-likelihood ratio (LLR) for different hypotheses to quantify the expected sensitivity across the mass range tested. Figure 4 displays the LLR distributions for the combined analyses as functions of m_H. Included are the median of the LLR distributions for the background-only hypothesis (LLR_b), the signal-plus-background hypothesis (LLR_{s+b}), and the observed value for the data ($\mathrm{LLR}_{\mathrm{obs}}$).

The shaded bands represent the one and two standard deviation (σ) departures for LLR_b centered on the median. At $m_H = 115$ GeV/c^2 a small excess in the data, at the 1- 2-sigma level, has the amplitude expected from a Higgs boson of this mass. Table VI lists the observed and expected LLR values shown in Figure 4.

These distributions can be interpreted as follows: The separation between the medians of the LLR_b and LLR_{s+b} distributions provides a measure of the discriminating power of the search. The sizes of the one- and two-σ LLR_b bands indicate the width of the LLR_b distribution, assuming no signal is truly present and only statistical fluctuations and systematic effects are present. The value of $\mathrm{LLR}_{\mathrm{obs}}$ relative to LLR_{s+b} and LLR_b indicates whether the data distribution appears to resemble what we expect if a signal is present (i.e. closer to the LLR_{s+b} distribution, which is negative by construction) or whether it resembles the background expectation more closely; the significance of any departures of $\mathrm{LLR}_{\mathrm{obs}}$ from LLR_b can be evaluated by the width of the LLR_b bands.

Using the combination procedures outlined in Section III, we extract limits on SM Higgs boson production $\sigma \times B(H \to X)$ in $p\bar{p}$ collisions at $\sqrt{s} = 1.96$ TeV for $100 \leq m_H \leq 200$ GeV/c^2. To facilitate comparisons with the standard model and to accommodate analyses with different degrees of sensitivity, we present our results in terms of the ratio of obtained limits to the SM Higgs boson production cross section, as a function of Higgs boson mass, for test masses for which both experiments have performed dedicated searches in different channels. A value of the combined limit ratio which is less than or equal to one indicates that that particular Higgs boson mass is excluded at the 95% C.L.

The combinations of results [1, 2] of each single experiment, as used in this Tevatron combination, yield the following ratios of 95% C.L. observed (expected) limits to the SM cross section: 1.55 (1.49) for CDF and 1.83 (1.90) for D0 at $m_H = 115$ GeV/c^2, 1.88 (1.55) for CDF and 2.42 (1.79) for D0 at $m_H = 140$ GeV/c^2, and 0.75 (0.79) for CDF and 0.71 (0.87) for D0 at $m_H = 165$ GeV/c^2.

The ratios of the 95% C.L. expected and observed limit to the SM cross section are shown in Figure 5 for the combined CDF and D0 analyses. The observed and median expected ratios are listed for the tested Higgs boson masses in Table IV for $m_H \leq 150$ GeV/c^2, and in Table V for $m_H \geq 155$ GeV/c^2, as obtained by the Bayesian and the $\mathrm{CL_s}$ methods. In the following summary we quote only the limits obtained with the Bayesian method, which was decided upon *a priori*. The corresponding limits and expected limits obtained using the $\mathrm{CL_s}$ method are shown alongside the Bayesian limits in the tables. We obtain the observed (expected) values of 0.68 (0.96) at $m_H = 105$ GeV/c^2, 1.17 (1.16) at $m_H = 115$ GeV/c^2, 1.71 (1.16) at $m_H = 140$ GeV/c^2, 1.08 (0.80) at $m_H = 155$ GeV/c^2, 0.48 (0.57) at $m_H = 165$ GeV/c^2, 0.91 (0.80) at $m_H = 175$ GeV/c^2, and 1.31 (1.22) at $m_H = 185$ GeV/c^2.

TABLE IV: Ratios of median expected and observed 95% C.L. limit to the SM cross section for the combined CDF and D0 analyses as a function of the Higgs boson mass in GeV/c^2, obtained with the Bayesian and with the $\mathrm{CL_s}$ method.

Bayesian	100	105	110	115	120	125	130	135	140	145	150
Expected	0.86	0.96	1.03	1.16	1.24	1.31	1.35	1.28	1.16	1.10	0.93
Observed	0.43	0.68	1.12	1.17	1.47	1.81	2.00	1.54	1.71	1.58	1.39
$\mathrm{CL_s}$	100	105	110	115	120	125	130	135	140	145	150
Expected	0.87	0.95	1.03	1.17	1.26	1.35	1.37	1.29	1.19	1.08	0.95
Observed	0.44	0.70	1.13	1.22	1.57	1.92	2.02	1.59	1.77	1.65	1.32

We also show in Figure 6 and list in Table VII the observed 1-$\mathrm{CL_s}$ and its expected distribution for the background-only hypothesis as a function of the Higgs boson mass. This is directly interpreted as the level of exclusion of our search. This figure is obtained using the $\mathrm{CL_s}$ method. We also show in Figure 6 $\mathrm{CL_s}$ as a function of m_H, which on a logarithmic scale more clearly shows the strength of the exclusion for values of m_H for which we have a large sensitivity. Figure 7 shows the p-value $\mathrm{CL_{s+b}}$ as a function of m_H and also $1 - \mathrm{CL_{s+b}}$, as well as the expected distributions in the absence of a Higgs boson signal.

We choose to use the intersections of piecewise linear interpolations of our observed and expected rate limits in order to quote ranges of Higgs boson masses that are excluded and that are expected to be excluded. The sensitivities of our searches to Higgs bosons are smooth functions of the Higgs boson mass and depend most strongly on the

predicted cross sections and the decay branching ratios (the decay $H \to W^+W^-$ is the dominant decay for the region of highest sensitivity). We therefore use the linear interpolations to extend the results from the 5 GeV/c^2 mass grid investigated to points in between. The regions of Higgs boson masses excluded at the 95% C.L. thus obtained are $156 < m_H < 177$ GeV/c^2 and $100 < m_H < 108$ GeV/c^2. The expected exclusion region, given the current sensitivity, is $148 < m_H < 180$ GeV/c^2 and $100 < m_H < 109$ GeV/c^2 (masses below $m_H < 100$ GeV/c^2 were not studied). The excluded region obtained by finding the intersections of the linear interpolations of the observed $1 - \mathrm{CL_s}$ curve shown in Figure 6 is nearly identical to that obtained with the Bayesian calculation. As previously stated, we make the *a priori* choice to quote the exclusion region using the Bayesian calculation.

We investigate the sensitivity and observed limits using CDF's and D0's searches for $H \to b\bar{b}$ taken in combination. These channels contribute the most for values of m_H below around 130 GeV/c^2. The contributing channels for CDF are the $WH \to \ell\nu b\bar{b}$ channels, the $ZH \to \nu\bar{\nu}b\bar{b}$ channels, the $ZH \to \ell^+\ell^- b\bar{b}$ channels, the $WH + ZH + VBF \to jjb\bar{b}$ channels, and all of the $t\bar{t}H$ channels. The contributing channels for D0 are the $WH \to \ell\nu b\bar{b}$ channels, the $ZH \to \nu\bar{\nu}b\bar{b}$

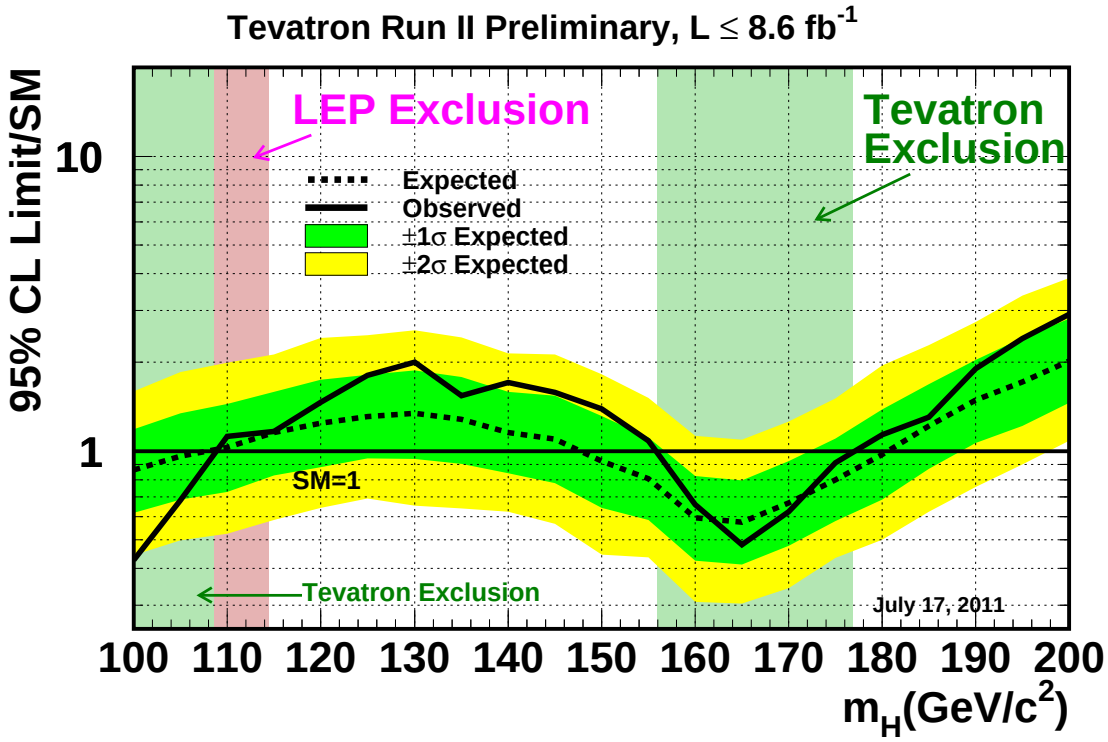

FIG. 5: Observed and expected (median, for the background-only hypothesis) 95% C.L. upper limits on the ratios to the SM cross section, as functions of the Higgs boson mass for the combined CDF and D0 analyses. The limits are expressed as a multiple of the SM prediction for test masses (every 5 GeV/c^2) for which both experiments have performed dedicated searches in different channels. The points are joined by straight lines for better readability. The bands indicate the 68% and 95% probability regions where the limits can fluctuate, in the absence of signal. The limits displayed in this figure are obtained with the Bayesian calculation.

TABLE V: Ratios of median expected and observed 95% C.L. limit to the SM cross section for the combined CDF and D0 analyses as a function of the Higgs boson mass in GeV/c^2, obtained with the Bayesian and with the CL_s method.

Bayesian	155	160	165	170	175	180	185	190	195	200
Expected	0.80	0.59	0.57	0.67	0.80	0.97	1.22	1.49	1.71	2.02
Observed	1.08	0.66	0.48	0.62	0.91	1.14	1.31	1.90	2.41	2.91

CL_s	155	160	165	170	175	180	185	190	195	200
Expected	0.82	0.61	0.58	0.67	0.81	0.98	1.24	1.50	1.77	2.04
Observed	1.03	0.67	0.48	0.61	0.92	1.17	1.34	1.92	2.39	2.82

channels, and the $ZH \to \ell^+\ell^- b\bar{b}$ channels. The result of this combination is shown in Figure 8.

In summary, we combine all available CDF and D0 results on SM Higgs boson searches, based on luminosities ranging from 4.0 to 8.6 fb^{-1}. Compared to our previous combination, more data have been added to the existing channels, additional channels have been included, and analyses have been further optimized to gain sensitivity. The results presented here significantly extend the individual limits of each collaboration and those obtained in our previous combination. The sensitivity of our combined search is sufficient to exclude a Higgs boson at high mass and is, in the absence of signal, expected to grow substantially in the future as more data are added and further improvements are made to our analysis techniques. We observe a small ($\approx 1\sigma$) excess in the range $125 < m_H < 155$ GeV/c^2 which does not allow exclusion of a Higgs boson to as low a mass as expected. In addition, we combine the CDF and D0 analyses which seek specifically the $H \to b\bar{b}$ decay, which dominates at the low end of the allowed mass range for the SM Higgs boson. These are the search modes for which we expect Tevatron sensitivity to remain competitive with the LHC experiments for several years to come.

TABLE VI: Log-likelihood ratio (LLR) values for the combined CDF + D0 Higgs boson search obtained using the CL_S method.

m_H (GeV/c^2	LLR_{obs}	LLR_{S+B}^{med}	$LLR_B^{-2\sigma}$	$LLR_B^{-1\sigma}$	LLR_B^{med}	$LLR_B^{+1\sigma}$	$LLR_B^{+2\sigma}$
100	13.03	-5.26	13.85	9.40	4.95	0.50	-3.95
105	7.96	-4.51	12.43	8.32	4.22	0.11	-4.00
110	2.43	-3.84	11.28	7.46	3.64	-0.17	-3.99
115	1.01	-2.98	9.59	6.21	2.84	-0.53	-3.90
120	0.24	-2.55	8.71	5.58	2.45	-0.68	-3.81
125	-1.11	-2.24	8.05	5.11	2.17	-0.78	-3.72
130	-1.94	-2.13	7.85	4.97	2.08	-0.80	-3.69
135	0.80	-2.43	8.50	5.43	2.36	-0.71	-3.78
140	-1.01	-2.84	9.35	6.05	2.74	-0.57	-3.88
145	-0.95	-3.41	10.59	6.95	3.31	-0.33	-3.97
150	0.14	-4.38	12.44	8.33	4.22	0.11	-4.00
155	1.68	-5.91	15.02	10.30	5.57	0.85	-3.87
160	7.82	-10.57	21.93	15.74	9.56	3.38	-2.81
165	13.23	-11.52	23.25	16.81	10.37	3.93	-2.51
170	9.00	-8.88	19.36	13.69	8.03	2.36	-3.31
175	4.14	-6.08	15.12	10.37	5.63	0.88	-3.86
180	1.86	-4.20	12.00	8.00	4.00	-0.00	-4.00
185	1.58	-2.63	8.92	5.73	2.54	-0.65	-3.84
190	-0.27	-1.85	7.13	4.46	1.78	-0.89	-3.56
195	-0.62	-1.33	5.85	3.57	1.30	-0.98	-3.26
200	-0.72	-1.02	4.97	2.98	0.99	-1.00	-2.99

Acknowledgments

We thank the Fermilab staff and the technical staffs of the participating institutions for their vital contributions, and we acknowledge support from the DOE and NSF (USA); CONICET and UBACyT (Argentina); ARC (Australia); CNPq, FAPERJ, FAPESP and FUNDUNESP (Brazil); CRC Program and NSERC (Canada); CAS, CNSF, and NSC (China); Colciencias (Colombia); MSMT and GACR (Czech Republic); Academy of Finland (Finland); CEA and CNRS/IN2P3 (France); BMBF and DFG (Germany); INFN (Italy); DAE and DST (India); SFI (Ireland); Ministry of Education, Culture, Sports, Science and Technology (Japan); KRF, KOSEF and World Class University Program (Korea); CONACyT (Mexico); FOM (The Netherlands); FASI, Rosatom and RFBR (Russia); Slovak R&D Agency (Slovakia); Ministerio de Ciencia e Innovación, and Programa Consolider-Ingenio 2010 (Spain); The Swedish Research Council (Sweden); Swiss National Science Foundation (Switzerland); STFC and the Royal Society (United Kingdom); and the A.P. Sloan Foundation (USA).

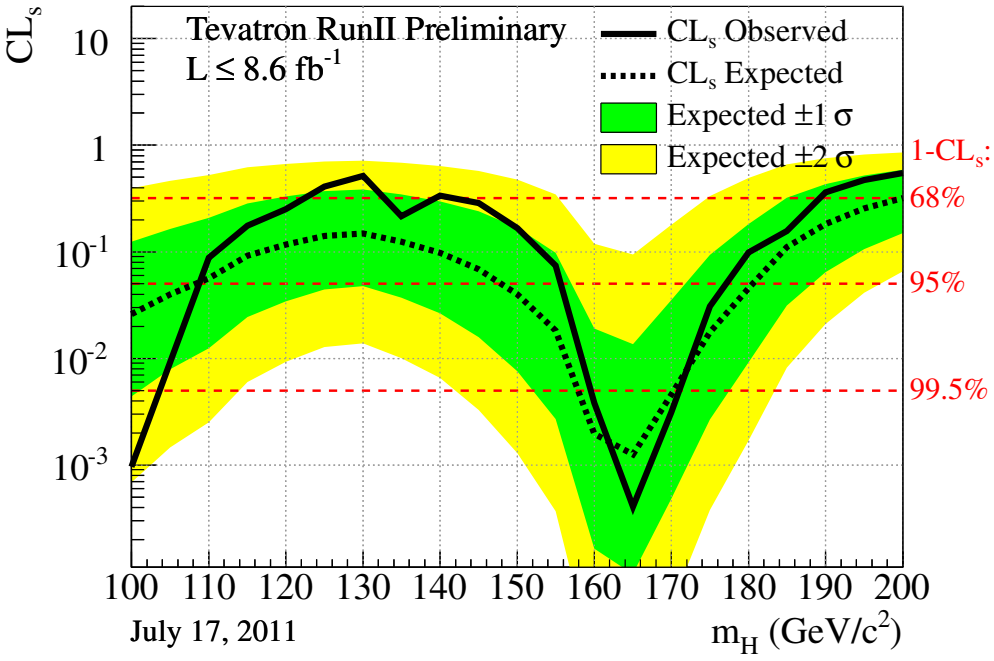

(a)

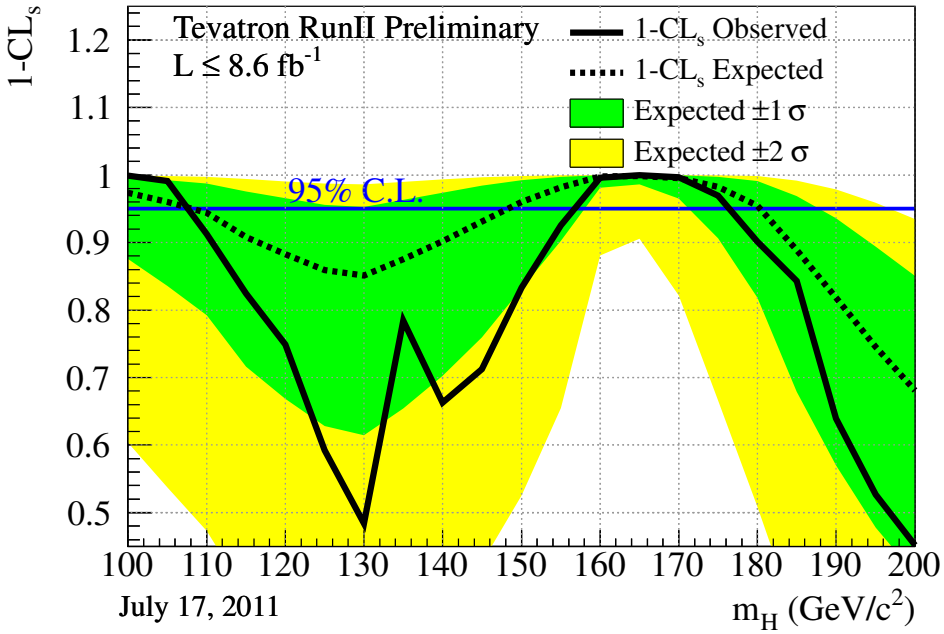

(b)

FIG. 6: The exclusion strength CL_s (a) and 1-CL_s (b) as functions of the Higgs boson mass (in steps of 5 GeV/c^2), for the combination of the CDF and D0 analyses. The green and yellow bands correspond to the regions enclosing 1-σ and 2-σ fluctuations of the background, respectively.

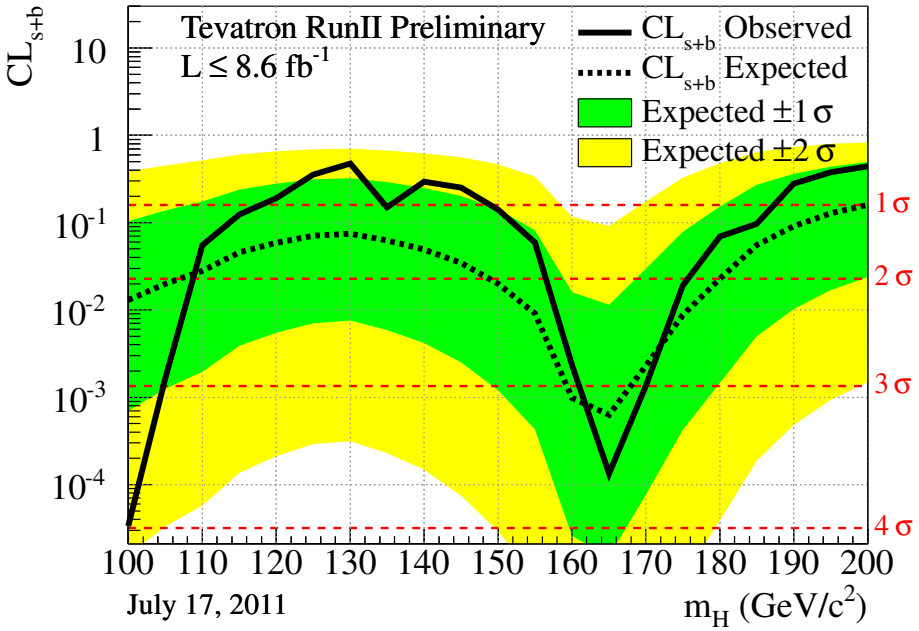

(a)

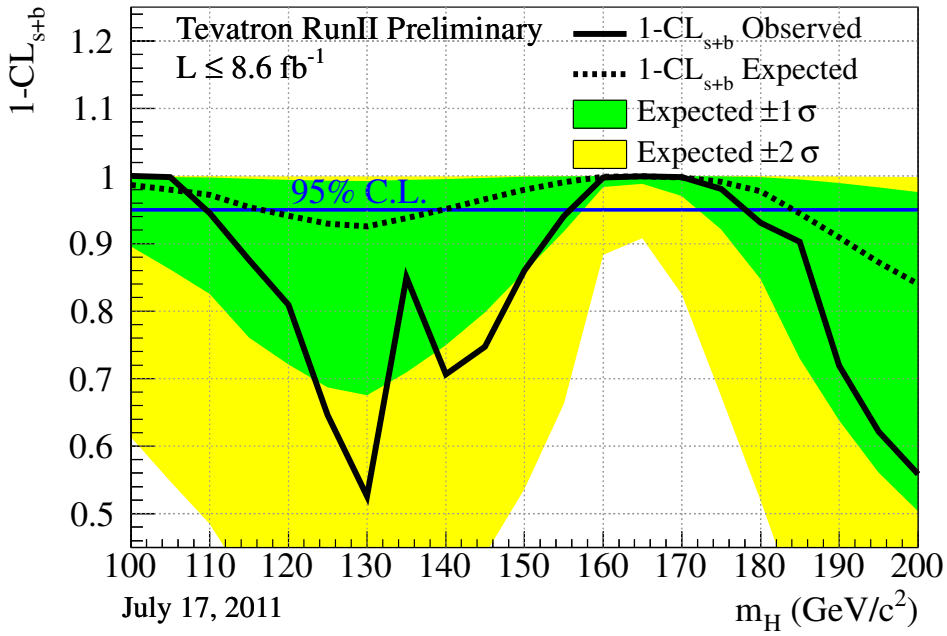

(b)

FIG. 7: The signal p-values CL_{s+b} (a) and 1-CL_{s+b} (b) as functions of the Higgs boson mass (in steps of 5 GeV/c^2), for the combination of the CDF and D0 analyses. The green and yellow bands correspond to the regions enclosing 1-σ and 2-σ fluctuations of the background, respectively.

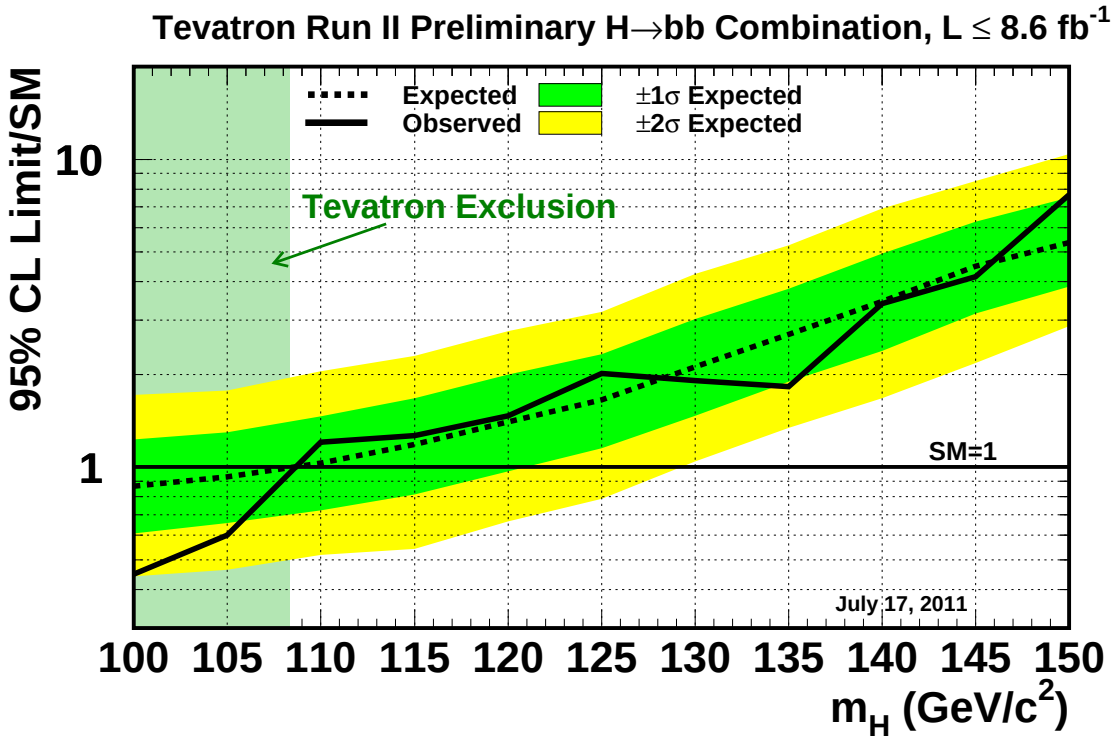

FIG. 8: Observed and expected (median, for the background-only hypothesis) 95% C.L. upper limits on the ratios to the SM cross section, as functions of the Higgs boson mass for the combination of CDF and D0 analyses focusing on the $H \to b\bar{b}$ decay channel. The limits are expressed as a multiple of the SM prediction for test masses (every 5 GeV/c^2) for which both experiments have performed dedicated searches in different channels. The points are joined by straight lines for better readability. The bands indicate the 68% and 95% probability regions where the limits can fluctuate, in the absence of signal. The limits displayed in this figure are obtained with the Bayesian calculation.

TABLE VII: The observed and expected 1-CL_s values as functions of m_H, for the combined CDF and D0 Higgs boson searches.

m_H (GeV/c^2)	1-CL_s^{obs}	1-$CL_s^{-2\sigma}$	1-$CL_s^{-1\sigma}$	1-CL_s^{median}	1-$CL_s^{+1\sigma}$	1-$CL_s^{+2\sigma}$
100	0.999	0.999	0.996	0.974	0.876	0.604
105	0.991	0.999	0.992	0.960	0.835	0.537
110	0.912	0.997	0.988	0.944	0.792	0.473
115	0.824	0.994	0.976	0.908	0.716	0.380
120	0.749	0.991	0.966	0.883	0.669	0.332
125	0.592	0.987	0.956	0.859	0.628	0.294
130	0.484	0.986	0.953	0.851	0.614	0.281
135	0.784	0.990	0.963	0.875	0.654	0.317
140	0.663	0.993	0.974	0.902	0.702	0.365
145	0.712	0.997	0.984	0.931	0.760	0.426
150	0.833	0.999	0.992	0.960	0.832	0.526
155	0.926	1.000	0.997	0.982	0.902	0.655
160	0.996	1.000	1.000	0.998	0.981	0.881
165	1.000	1.000	1.000	0.999	0.986	0.906
170	0.997	1.000	1.000	0.995	0.965	0.821
175	0.969	1.000	0.997	0.982	0.906	0.666
180	0.901	0.998	0.991	0.955	0.818	0.508
185	0.843	0.992	0.969	0.889	0.679	0.341
190	0.639	0.979	0.936	0.818	0.570	0.247
195	0.527	0.959	0.894	0.745	0.478	0.184
200	0.451	0.934	0.851	0.681	0.410	0.145

[1] CDF Collaboration, "Combined Upper Limit on Standard Model Higgs Boson Production for EPS2011",CDF Conference Note 10609 (2011).

[2] "Combined Upper Limits on Standard Model Higgs Boson Production from the D0 Experiment in up to 8.6 fb^{-1} of data", D0 Conference Note 6229 (2011).

[3] The CDF and D0 Collaborations and the TEVNPH Working Group, "Combined CDF and D0 Upper Limits on Standard Model Higgs Boson Production with up to 8.2 fb^{-1} of Data,", FERMILAB-CONF-11-044-E, CDF Note 10441, D0 Note 6184, arXiv:1103.3233v1 [hep-ex] (2011);
The CDF and D0 Collaborations and the TEVNPH Working Group, "Combined CDF and D0 Upper Limits on Standard Model Higgs-Boson Production with up to 6.7 fb^{-1} of Data", FERMILAB-CONF-10-257-E, CDF Note 10241, D0 Note 6096, arXiv:1007.4587v1 [hep-ex] (2010);
The CDF and D0 Collaborations and the TEVNPH Working Group, "Combined CDF and DZero Upper Limits on Standard Model Higgs-Boson Production with 2.1 to 4.2 fb^{-1} of Data", FERMILAB-PUB-09-0557-E, CDF Note 9998, D0 Note 5983, arXiv:0911.3930v1 [hep-ex] (2009).
CDF Collaboration, "Search for $H \to WW^*$ Production Using 5.9 fb^{-1}", CDF Conference Note 10432 (2011);
CDF Collaboration, "Combined Upper Limit on Standard Model Higgs Boson Production for ICHEP 2010",CDF Conference Note 10241 (2010);
CDF Collaboration, "Combined Upper Limit on Standard Model Higgs Boson Production for HCP 2009", CDF Conference Note 9999 (2009);
CDF Collaboration, "Combined Upper Limit on Standard Model Higgs Boson Production for Summer 2009", CDF Conference Note 9807 (2009);
D0 Collaboration, "Combined Upper Limits on Standard Model Higgs Boson Production in the W^+W^-, $\tau\tau$ and $\gamma\gamma$ decay modes from the D0 Experiment in up to 8.2 fb^{-1} of data", D0 Conference Note 6183 (2011);
D0 Collaboration, "Combined Upper Limits on Standard Model Higgs Boson Production from the D0 Experiment in up to 6.7 fb^{-1} of data", D0 Conference Note 6094 (2010);
D0 Collaboration,"Combined Upper Limits on Standard Model Higgs Boson Production from the D0 Experiment in 2.1-5.4 fb^{-1}", D0 Conference Note 6008 (2009);
D0 Collaboration, "Combined upper limits on Standard Model Higgs boson production from the D0 experiment in 0.9-5.0 fb^{-1}", D0 Conference Note 5984 (2009).

[4] CDF Collaboration, " Inclusive Search for Standard Model Higgs Boson Production in the WW Decay Channel Using the CDF II Detector", Phys. Rev. Lett. 104, 061803 (2010);
D0 Collaboration, " Search for Higgs Boson Production in Dilepton and Missing Energy Final States with 5.4 fb^{-1} of $p\bar{p}$ Collisions at $\sqrt{s} = 1.96$ TeV", Phys. Rev. Lett. 104, 061804 (2010);
The CDF and D0 Collaborations, "Combination of Tevatron Searches for the Standard Model Higgs Boson in the W^+W^- Decay Mode", Phys. Rev. Lett. 104, 061802 (2010).

[5] CDF Collaboration, "Search for standard model Higgs boson production in association with a W boson with 7.5 fb^{-1}", CDF Conference Note 10596 (2011).

[6] CDF Collaboration, "Search for standard model Higgs boson production in association with a W boson using Matrix Element techniques with 5.6 fb^{-1} of CDF Data", CDF Conference Note 10217 (2010).

[7] CDF Collaboration, "Search for the standard model Higgs boson in the $\not\!\!E_T$ plus b-jets signature in 7.8 fb^{-1}", CDF Conference Note 10583 (2011).

[8] CDF Collaboration, "A Search for the standard model Higgs boson in the process $ZH \to e^+e^-b\bar{b}$ using 7.5 fb^{-1} of CDF II Data", CDF Conference Note 10593 (2011).

[9] CDF Collaboration, "Search for the standard model Higgs boson in the $ZH \to \mu^+\mu^-b\bar{b}$ final state using 7.9 fb^{-1}", CDF Conference Note 10572 (2011).

[10] CDF Collaboration, "Search for $H \to WW^*$ Production Using 8.2 fb^{-1}", CDF Conference Note 10599 (2011).

[11] CDF Collaboration, "A search for the Higgs boson in the four lepton final state", CDF Conference Note 10573 (2011).

[12] CDF Collaboration, "Search for a low mass standard model Higgs boson in the di-tau decay channel using 6.0 fb^{-1}", CDF Conference Note 10439 (2011).

[13] CDF Collaboration, "Search for the standard model Higgs in the $\ell\nu\tau\tau$ and $\ell\ell\tau\tau$ channels", CDF Conference Note 10500 (2011).

[14] CDF Collaboration, "A search for the Higgs Boson in the All Hadronic Channel with Data Sample of 4 fb^{-1}", CDF Conference Note 10010 (2010).

[15] CDF Collaboration, "Search for a standard model Higgs boson decaying into photons at CDF using 6.0 fb^{-1} of data",

CDF Conference Note 10485 (2011).
[16] CDF Collaboration, "Search for the Higgs boson produced in association with top quarks", CDF Conference Note 10574 (2011).
[17] CDF Collaboration, "Search for standard model Higgs boson production in association with $t\bar{t}$ using no lepton final state", CDF Conference Note 10582 (2011).
[18] D0 Collaboration, "Search for WH associated production with 8.5 fb^{-1} of Tevatron data," D0 Conference Note 6220.
[19] D0 Collaboration, "Search for the standard model Higgs boson in the $ZH \to b\bar{b}\nu\nu$ channel in 8.4 fb^{-1} of $p\bar{p}$ collisions at $\sqrt{s} = 1.96$ TeV", D0 Conference note 6223.
[20] D0 Collaboration, "A Search for $ZH \to \ell^+\ell^- b\bar{b}$ Production in 8.6 fb^{-1} of $p\bar{p}$ Collisions", D0 Conference Note 6166.
[21] D0 Collaboration, "Search for the standard model Higgs boson in the $\tau^+\tau^- + 2$ jets final state", D0 Conference note 6171.
[22] D0 Collaboration, "Search for associated Higgs boson production using like charge dilepton events in $p\bar{p}$ collisions at $\sqrt{s} = 1.96$ TeV", [e-Print: arXiv:1107.1268v1 [hep-ph]].
[23] D0 Collaboration, " Search for Higgs boson production in dilepton plus missing energy final states with 8.1 fb^{-1} of $p\bar{p}$ collisions at $\sqrt{s} = 1.96$ TeV", D0 Conference Note 6219.
[24] D0 Collaboration, " Search for the Standard Model Higgs boson in $\mu + \tau_{\rm had} \leq 1$ jet final state with 7.3 fb^{-1} of data", D0 Conference Note 6179.
[25] D0 Collaboration, "A search for the standard model Higgs boson in the $H \to WW \to \ell\nu q\bar{q}'$ Decay Channel", Phys. Rev. Lett. 106, 171802 (2011)
[26] D0 Collaboration, "Search for the Standard Model Higgs boson in $\gamma\gamma$ final states at D0 with 8.2 fb^{-1} of data", D0 Conference Note 6177.
[27] V. M. Abazov *et al.* [The D0 Collaboration], Nucl. Instrum. Meth. A **620**, 490 (2010).
[28] A. Hoecker, P. Speckmayer, J. Stelzer, J.Therhaag, E. von Toerne, and H. Voss, "TMVA 4 Toolkit for Multivariate Data Analysis with ROOT User's Guide" arXiv:physics/0703039a;
C. Cortes and V. Vapnik, "Support vector networks", Machine Learning **20**, 273 (1995);
V. Vapnik, "The Nature of Statistical Learning Theory", Springer Verlag, New York (1995);
C.J.C. Burges, "A Tutorial on Support Vector Machines for Pattern Recognition", Data Mining and Knowledge Disovery **2**, 1 (1998).
[29] T. Sjöstrand, L. Lonnblad and S. Mrenna, "PYTHIA 6.2: Physics and manual," arXiv:hep-ph/0108264.
[30] M. L. Mangano, M. Moretti, F. Piccinini, R. Pittau and A. D. Polosa, "ALPGEN, a generator for hard multiparton processes in hadronic collisions," JHEP **0307**, 001 (2003).
[31] S. Frixione and B.R. Webber, JHEP **0206**, 029 (2002).
[32] G. Corcella *et al.*, JHEP **0101**, 010 (2001).
[33] A. Pukhov *et al.*, "CompHEP: A package for evaluation of Feynman diagrams and integration over multi-particle phase space. User's manual for version 33," [arXiv:hep-ph/9908288].
[34] J. Campbell and R. K. Ellis, http://mcfm.fnal.gov/.
[35] C. Anastasiou, R. Boughezal and F. Petriello, JHEP **0904**, 003 (2009).
[36] D. de Florian and M. Grazzini, Phys. Lett. B **674**, 291 (2009).
[37] M. Grazzini, private communication (2010).
[38] The CDF and D0 Collaborations and the Tevatron Electroweak Working Group, arXiv:0903.2503 [hep-ex].
[39] R. V. Harlander and W. B. Kilgore, Phys. Rev. Lett. **88**, 201801 (2002).
[40] C. Anastasiou and K. Melnikov, Nucl. Phys. B **646**, 220 (2002).
[41] V. Ravindran, J. Smith, and W. L. van Neerven, Nucl. Phys. B **665**, 325 (2003).
[42] S. Actis, G. Passarino, C. Sturm, and S. Uccirati, Phys. Lett. B **670**, 12 (2008).
[43] U. Aglietti, R. Bonciani, G. Degrassi, A. Vicini, "Two-loop electroweak corrections to Higgs production in proton-proton collisions", arXiv:hep-ph/0610033v1 (2006).
[44] S. Catani, D. de Florian, M. Grazzini and P. Nason, "Soft-gluon resummation for Higgs boson production at hadron colliders," JHEP **0307**, 028 (2003) [arXiv:hep-ph/0306211].
[45] A. D. Martin, W. J. Stirling, R. S. Thorne and G. Watt, Eur. Phys. J. C **63**, 189 (2009).
[46] `http://www.hep.ucl.ac.uk/pdf4lhc/`;
S. Alekhin *et al.*, (PDF4LHC Working Group), [arXiv:1101.0536v1 [hep-ph]];
M. Botje *et al.*, (PDF4LHC Working Group), [arXiv:1101.0538v1 [hep-ph]].
[47] I. W. Stewart, F. J. Tackmann, [arXiv:1107.2117 [hep-ph]].
[48] C. Anastasiou, G. Dissertori, M. Grazzini, F. Stöckli and B. R. Webber, JHEP **0908**, 099 (2009).
[49] J. M. Campbell, R. K. Ellis, C. Williams, Phys. Rev. **D81**, 074023 (2010). [arXiv:1001.4495 [hep-ph]].
[50] G. Bozzi, S. Catani, D. de Florian, and M. Grazzini, Phys. Lett. B **564**, 65 (2003);
G. Bozzi, S. Catani, D. de Florian, and M. Grazzini, Nucl. Phys. B **737**, 73 (2006).

[51] C. Balazs, J. Huston, I. Puljak, Phys. Rev. D **63** 014021 (2001).
C. Balazs and C.-P. Yuan, Phys. Lett. B **478** 192-198 (2000).
Qing-Hong Cao and Chuan-Ren Chen, Phys. Rev. D **76** 073006 (2007).

[52] J. Baglio and A. Djouadi, arXiv:1003.4266 [hep-ph] (2010). We have obtained extended versions of the table of WH and ZH cross sections for all Higgs boson masses we test, and with more digits of precision, from the authors.

[53] The Fortran program can be found on Michael Spira's web page `http://people.web.psi.ch/~mspira/proglist.html`.

[54] O. Brein, A. Djouadi, and R. Harlander, Phys. Lett. B **579**, 149 (2004).

[55] M. L. Ciccolini, S. Dittmaier, and M. Kramer, Phys. Rev. D **68**, 073003 (2003).

[56] P. Bolzoni, F. Maltoni, S.-O. Moch, and M. Zaro, Phys. Rev. Lett. **105**, 011801 (2010) [arXiv:1003.4451v2 [hep-ph]].

[57] M. Ciccolini, A. Denner, and S. Dittmaier, Phys. Rev. Lett. **99**, 161803 (2007) [arXiv:0707.0381 [hep-ph]];
M. Ciccolini, A. Denner, and S. Dittmaier, Phys. Rev. D **77**, 013002 (2008) [arXiv:0710.4749 [hep-ph]].
We would like to thank the authors of the HAWK program for adapting it to the Tevatron.

[58] W. Beenaker, S. Dittmaier, M. Krämer, B. Plümper, M. Spira, and P. M. Zerwas, Phys. Rev. Lett. **87**, 201805 (2001);
L. Reina and S. Dawson, Phys. Rev. Lett. **87**, 201804 (2001).

[59] H. L. Lai *et al.*, Phys. Rev D **55**, 1280 (1997).

[60] S. Dittmaier *et al.* [LHC Higgs Cross Section Working Group Collaboration], [arXiv:1101.0593 [hep-ph]].

[61] A. Djouadi, J. Kalinowski and M. Spira, Comput. Phys. Commun. **108**, 56 (1998).

[62] A. Bredenstein, A. Denner, S. Dittmaier, and M. M. Weber, Phys. Rev. D **74**, 013004 (2006);
A. Bredenstein, A. Denner, S. Dittmaier, and M. Weber, JHEP **0702**, 080 (2007);
A. Bredenstein, A. Denner, S. Dittmaier, A. Mück, and M. M. Weber, JHEP **0702**, 080 (2007) `http://omnibus.uni-freiburg.de/~sd565/programs/prophycey4f/prophecy4f.html` (2010).

[63] J. Baglio, A. Djouadi, JHEP **1103**, 055 (2011). [arXiv:1012.0530 [hep-ph]].

[64] T. Junk, Nucl. Instrum. Meth. A **434**, 435 (1999);
A.L. Read, "Modified Frequentist analysis of search results (the CL_s method)", in F. James, L. Lyons and Y. Perrin (eds.), *Workshop on Confidence Limits*, CERN, Yellow Report 2000-005, available through `cdsweb.cern.ch`.

[65] W. Fisher, "Systematics and Limit Calculations," FERMILAB-TM-2386-E.

[66] S. Moch and P. Uwer, U. Langenfeld, S. Moch and P. Uwer, Phys. Rev. D **80**, 054009 (2009).

[67] M. Cacciari, S. Frixione, M. L. Mangano, P. Nason and G. Ridolfi, JHEP **0809**, 127 (2008).
N. Kidonakis and R. Vogt, Phys. Rev. D **78**, 074005 (2008).

[68] N. Kidonakis, Phys. Rev. D **74**, 114012 (2006).

[69] N. Kidonakis, private communication.

[70] N. Kidonakis, arXiv:1005.3330 [hep-ph].

[71] B. W. Harris, E. Laenen, L. Phaf, Z. Sullivan and S. Weinzierl, Phys. Rev. D **66**, 054024 (2002).

[72] J. Campbell and R. K. Ellis, Phys. Rev. D **65**, 113007 (2002).

Appendices

APPENDIX A: SYSTEMATIC UNCERTAINTIES

TABLE VIII: Systematic uncertainties on the signal and background contributions for CDF's $WH \to \ell\nu b\bar{b}$ tight double tag (TDT), loose double tag (LDT), looser double tag (LDTX), and single tag (ST) 2 jet channels. Systematic uncertainties are listed by name; see the original references for a detailed explanation of their meaning and on how they are derived. Systematic uncertainties for WH shown in this table are obtained for $m_H = 115$ GeV/c^2. Uncertainties are relative, in percent, and are symmetric unless otherwise indicated. Shape uncertainties are labeled with an "S".

CDF: tight and loose double-tag (TDT and LDT) $WH \to \ell\nu b\bar{b}$ channel relative uncertainties (%)

Contribution	W+HF	Mistags	Top	Diboson	Non-W	WH
Luminosity ($\sigma_{\rm inel}(p\bar{p})$)	3.8	0	3.8	3.8	0	3.8
Luminosity Monitor	4.4	0	4.4	4.4	0	4.4
Lepton ID	2.0-4.5	0	2.0-4.5	2.0-4.5	0	2.0-4.5
Jet Energy Scale	S	0	S	S	0	2(S)
Mistag Rate	0	35	0	0	0	0
B-Tag Efficiency	8.6	0	8.6	8.6	0	8.6
$t\bar{t}$ Cross Section	0	0	10	0	0	0
Diboson Rate	0	0	0	11.5	0	0
Signal Cross Section	0	0	0	0	0	5
HF Fraction in W+jets	45	0	0	0	0	0
ISR+FSR+PDF	5.0-7.7	0	5.0-7.7	5.0-7.7	0	5.0-7.7
Q^2	S	0	0	0	0	0
QCD Rate	0	0	0	0	40	0

CDF: looser double-tag (LDTX) $WH \to \ell\nu b\bar{b}$ channel relative uncertainties (%)

Contribution	W+HF	Mistags	Top	Diboson	Non-W	WH
Luminosity ($\sigma_{\rm inel}(p\bar{p})$)	3.8	0	3.8	3.8	0	3.8
Luminosity Monitor	4.4	0	4.4	4.4	0	4.4
Lepton ID	2.0-4.5	0	2.0-4.5	2.0-4.5	0	2.0-4.5
Jet Energy Scale	S		S	S		2.2(S)
Mistag Rate	0	36	0	0	0	0
B-Tag Efficiency	13.6	0	13.6	13.6	0	13.6
$t\bar{t}$ Cross Section	0	0	10	0	0	0
Diboson Rate	0	0	0	11.5	0	0
Signal Cross Section	0	0	0	0	0	5
HF Fraction in W+jets	45	0	0	0	0	0
ISR+FSR+PDF	4.9-19.5	0	4.9-19.5	4.9-19.5	0	4.9-19.5
Q^2	S	0	0	0	0	0
QCD Rate	0	0	0	0	40	0

CDF: single tag (ST) $WH \to \ell\nu b\bar{b}$ channel relative uncertainties (%)

Contribution	W+HF	Mistags	Top	Diboson	Non-W	WH
Luminosity ($\sigma_{\rm inel}(p\bar{p})$)	3.8	0	3.8	3.8	0	3.8
Luminosity Monitor	4.4	0	4.4	4.4	0	4.4
Lepton ID	2.0-4.5	0	2.0-4.5	2.0-4.5	0	2.0-4.5
Jet Energy Scale	S	0	S	S	0	2.3-4.7(S)
Mistag Rate	0	35	0	0	0	0
B-Tag Efficiency	4.3	0	4.3	4.3	0	4.3
$t\bar{t}$ Cross Section	0	0	10	0	0	0
Diboson Rate	0	0	0	11.5	0	0
Signal Cross Section	0	0	0	0	0	5
HF Fraction in W+jets	42	0	0	0	0	0
ISR+FSR+PDF	3.0-8.4	0	3.0-8.4	3.0-8.4	0	3.0-8.4
Q^2	S	0	0	0	0	0
QCD Rate	0	0	0	0	40	0

TABLE IX: Systematic uncertainties on the signal and background contributions for CDF's $WH \to \ell\nu b\bar{b}$ tight double tag (TDT), loose double tag (LDT), and single tag (ST) 3 jet channels. Systematic uncertainties are listed by name; see the original references for a detailed explanation of their meaning and on how they are derived. Systematic uncertainties for WH shown in this table are obtained for $m_H = 115$ GeV/c^2. Uncertainties are relative, in percent, and are symmetric unless otherwise indicated. Shape uncertainties are labeled with an "S".

CDF: tight and loose double-tag (TDT and LDT) $WH \to \ell\nu b\bar{b}$ channel relative uncertainties (%)

Contribution	W+HF	Mistags	Top	Diboson	Non-W	WH
Luminosity ($\sigma_{\rm inel}(p\bar{p})$)	3.8	0	3.8	3.8	0	3.8
Luminosity Monitor	4.4	0	4.4	4.4	0	4.4
Lepton ID	2	0	2	2	0	2
Jet Energy Scale	S	0	S	0	0	13.5(S)
Mistag Rate	0	9	0	0	0	0
B-Tag Efficiency	8.4	0	8.4	8.4	0	8.4
$t\bar{t}$ Cross Section	0	0	10	0	0	0
Diboson Rate	0	0	0	10	0	0
Signal Cross Section	0	0	0	0	0	10
HF Fraction in W+jets	30	0	0	0	0	0
ISR+FSR+PDF	21.4	0	21.4	21.4	0	21.4
QCD Rate	0	0	0	0	40	0

CDF: single tag (ST) $WH \to \ell\nu b\bar{b}$ channel relative uncertainties (%)

Contribution	W+HF	Mistags	Top	Diboson	Non-W	WH
Luminosity ($\sigma_{\rm inel}(p\bar{p})$)	3.8	0	3.8	3.8	0	3.8
Luminosity Monitor	4.4	0	4.4	4.4	0	4.4
Lepton ID	2	0	2	2	0	2
Jet Energy Scale	S	0	S	0	0	15.8(S)
Mistag Rate	0	13.3	0	0	0	0
B-Tag Efficiency	3.5	0	3.5	3.5	0	3.5
$t\bar{t}$ Cross Section	0	0	10	0	0	0
Diboson Rate	0	0	0	10	0	0
Signal Cross Section	0	0	0	0	0	10
HF Fraction in W+jets	30	0	0	0	0	0
ISR+FSR+PDF	13.1	0	13.1	13.1	0	13.1
QCD Rate	0	0	0	0	40	0

TABLE X: Systematic uncertainties on the signal and background contributions for D0's $WH \to \ell\nu b\bar{b}$ loose single (LST) and double tag (LDT) channels. Systematic uncertainties are listed by name, see the original references for a detailed explanation of their meaning and on how they are derived. Systematic uncertainties for WH shown in this table are obtained for $m_H = 115$ GeV/c^2. Uncertainties are relative, in percent, and are symmetric unless otherwise indicated. Shape uncertainties are labeled with an "S", and "SH" represents a shape-only uncertainty.

D0: single tag (ST) $WH \to \ell\nu b\bar{b}$ channel relative uncertainties (%)

Contribution	WZ/WW	Wbb/Wcc	Wjj/Wcj	$t\bar{t}$	single top	Multijet	WH
Luminosity	6.1	6.1	6.1	6.1	6.1	0	6.1
EM ID/Trigger eff. (S)	1–5	2–4	2–4	1–2	1–2	0	2–3
Muon Trigger eff. (S)	1–3	1–2	1–3	2–5	2–3	0	2–4
Muon ID/Reco eff./resol.	4.1	4.1	4.1	4.1	4.1	0	4.1
Jet ID/Reco eff. (S)	2–5	1–2	1–3	3–5	2–4	0	2–4
Jet Resolution (S)	4–7	1–3	1–4	2–5	2–4	0	4–6
Jet Energy Scale (S)	4–7	2–5	2–5	2–5	2–4	0	2–5
Vertex Conf. Jet (S)	4–10	5–12	4–10	7–10	5–10	0	4–8
b-tag/taggability (S)	1–4	1–2	3–7	3–5	1–2	0	1–2
Heavy-Flavor K-factor	0	20	0	0	0	0	0
Inst.-WH $e\nu b\bar{b}$ (S)	1–2	2–4	1–3	1–2	1–3	-15	1–2
Inst.-WH $\mu\nu b\bar{b}$	0	2.4	2.4	0	0	-20	0
Cross Section	6	9	9	10	10	0	6
Signal Branching Fraction	0	0	0	0	0	0	1-9
ALPGEN MLM pos/neg(S)	0	SH	0	0	0	0	0
ALPGEN Scale (S)	0	SH	SH	0	0	0	0
Underlying Event (S)	0	SH	0	0	0	0	0
PDF, reweighting	2	2	2	2	2	0	2

D0: double tag (DT) $WH \to \ell\nu b\bar{b}$ channel relative uncertainties (%)

Contribution	WZ/WW	Wbb/Wcc	Wjj/Wcj	$t\bar{t}$	single top	Multijet	WH
Luminosity	6.1	6.1	6.1	6.1	6.1	0	6.1
EM ID/Trigger eff. (S)	2–5	2–3	2–3	1–2	1–2	0	1–2
Muon Trigger eff. (S)	2–4	1–2	1–2	2–4	1–3	0	2–5
Muon ID/Reco eff./resol.	4.1	4.1	4.1	4.1	4.1	0	4.1
Jet ID/Reco eff. (S)	2–8	2–5	4–9	3–7	2–4	0	3–7
Jet Resolution (S)	4–7	2–7	2–7	2–9	2–4	0	4–6
Jet Energy Scale (S)	4–7	2–6	2–7	2–6	2–7	0	4–6
Vertex Conf. Jet (S)	4–10	5–12	4–10	7–10	5–10	0	4–6
b-tag/taggability (S)	3–7	4–6	3–10	5–10	4–10	0	4–9
Heavy-Flavor K-factor	0	20	0	0	0	0	0
Inst.-WH $e\nu b\bar{b}$ (S)	1–2	2–4	1–3	1–2	1–3	-15	1–2
Inst.-WH $\mu\nu b\bar{b}$	0	2.4	2.4	0	0	-20	0
Cross Section	6	9	9	10	10	0	6
Signal Branching Fraction	0	0	0	0	0	0	1-9
ALPGEN MLM pos/neg(S)	0	SH	0	0	0	0	0
ALPGEN Scale (S)	0	SH	SH	0	0	0	0
Underlying Event (S)	0	SH	0	0	0	0	0
PDF, reweighting	2	2	2	2	2	0	2

TABLE XI: Systematic uncertainties on the signal and background contributions for D0's $\tau\tau jj$ Run IIb channel. Systematic uncertainties for the Higgs signal shown in this table are obtained for $m_H = 135$ GeV/c^2. Systematic uncertainties are listed by name; see the original references for a detailed explanation of their meaning and on how they are derived. Uncertainties are relative, in percent, and are symmetric unless otherwise indicated. A systematic is denoted as flat if it affects the normalization only, and as a shape "S" uncertainty otherwise.

D0: $\mu\tau_{\rm had}jj$ Run IIb channel relative uncertainties (%)

Contribution	VH Signal	VBF Signal	ggH Signal	$W+jets$	$Z+jets$	Top	diboson	Multijet
Luminosity (D0 specific)	4.1	4.1	4.1	4.1	4.1	4.1	4.1	-
Luminosity (Tevatron common)	4.6	4.6	4.6	4.6	4.6	4.6	4.6	-
μ ID	2.9	2.9	2.9	2.9	2.9	2.9	2.9	-
μ trigger	8.6	8.6	8.6	8.6	8.6	8.6	8.6	-
τ energy correction	9.8	9.8	9.8	9.8	9.8	9.8	9.8	-
τ track efficiency	1.4	1.4	1.4	1.4	1.4	1.4	1.4	-
τ selection by type	12,4.2,7	12,4.2,7	12,4.2,7	12,4.2,7	12,4.2,7	12,4.2,7	12,4.2,7	-
Cross section	6.2	4.9	33	6.0	6.0	10.0	7.0	-
ggH Signal PDF	-	-	29	-	-	-	-	-
ggH Hp_T Reweighting (S)	1.0	1.0	1.0	1.0	1.0	1.0	1.0	-
Signal Branching Fraction	0-7.3	0-7.3	0-7.3	-	-	-	-	-
Vertex confirmation for jets	4.0	4.0	4.0	4.0	4.0	4.0	4.0	-
Jet ID(S)	∼10	∼10	∼10	∼10	∼10	∼10	∼10	-
Jet Energy Resolution (S)	∼10	∼10	∼10	∼10	∼10	∼10	∼10	-
Jet energy Scale (S)	∼15	∼15	∼15	∼15	∼15	∼15	∼15	-
Jet pT	5.5	5.5	5.5	5.5	5.5	5.5	5.5	-
PDF reweighting	2	2	2	2	2	2	2	-
Multijet Normalization	-	-	-	-	-	-	-	5.3
Multijet Shape	-	-	-	-	-	-	-	∼15

D0: $e\tau_{\rm had}jj$ Run IIb relative uncertainties (%)

Contribution	VH Signal	VBF Signal	ggH Signal	$W+jets$	$Z+jets$	Top	diboson	Multijet
Luminosity (D0 specific)	4.1	4.1	4.1	4.1	4.1	4.1	4.1	-
Luminosity (Tevatron common)	4.6	4.6	4.6	4.6	4.6	4.6	4.6	-
EM ID	4	4	4	4	4	4	4	-
e trigger	2	2	2	2	2	2	2	-
τ energy correction	9.8	9.8	9.8	9.8	9.8	9.8	9.8	-
τ track efficiency	1.4	1.4	1.4	1.4	1.4	1.4	1.4	-
τ selection by type	12,4.2,7	12,4.2,7	12,4.2,7	12,4.2,7	12,4.2,7	12,4.2,7	12,4.2,7	-
Cross section	6.2	4.9	33	6.0	6.0	10.0	7.0	-
ggH Signal PDF	-	-	29	-	-	-	-	-
ggH Hp_T Reweighting (S)	1.0	1.0	1.0	1.0	1.0	1.0	1.0	-
Signal Branching Fraction	0-7.3	0-7.3	0-7.3	-	-	-	-	-
Vertex confirmation for jets	4.0	4.0	4.0	4.0	4.0	4.0	4.0	-
Jet ID(S)	∼10	∼10	∼10	∼10	∼10	∼10	∼10	-
Jet Energy Resolution (S)	∼10	∼10	∼10	∼10	∼10	∼10	∼10	-
Jet energy Scale (S)	∼15	∼15	∼15	∼15	∼15	∼15	∼15	-
Jet pT	5.5	5.5	5.5	5.5	5.5	5.5	5.5	-
PDF reweighting	2	2	2	2	2	2	2	-
Multijet Normalization	-	-	-	-	-	-	-	4.7
Multijet Shape	-	-	-	-	-	-	-	∼15

TABLE XII: Systematic uncertainties on the signal and background contributions for CDF's $WH, ZH \to \not\!\!E_T b\bar{b}$ tight double tag (TDT), loose double tag (LDT), and single tag (ST) channels. Systematic uncertainties are listed by name; see the original references for a detailed explanation of their meaning and on how they are derived. Systematic uncertainties for ZH and WH shown in this table are obtained for $m_H = 120$ GeV/c^2. Uncertainties are relative, in percent, and are symmetric unless otherwise indicated. Shape uncertainties are labeled with an "S".

CDF: tight double-tag (TDT) $WH, ZH \to \not\!\!E_T b\bar{b}$ channel relative uncertainties (%)

Contribution	ZH	WH	Multijet	Mistags	Top Pair	S. Top	Di-boson	W + HF	Z + HF
Luminosity	3.8	3.8			3.8	3.8	3.8	3.8	3.8
Lumi Monitor	4.4	4.4			4.4	4.4	4.4	4.4	4.4
Tagging SF	10.4	10.4			10.4	10.4	10.4	10.4	10.4
Trigger Eff. (S)	0.9	1.4	0.9		0.9	1.6	2.0	1.8	1.2
Lepton Veto	2.0	2.0			2.0	2.0	2.0	2.0	2.0
PDF Acceptance	3.0	3.0			3.0	3.0	3.0	3.0	3.0
JES (S)	$^{+1.7}_{-1.8}$	$^{+2.4}_{-2.3}$			$^{+0.0}_{-0.1}$	$^{+2.5}_{-2.4}$	$^{+4.1}_{-4.5}$	$^{+4.3}_{-4.6}$	$^{+8.8}_{-3.2}$
ISR/FSR	$^{+3.0}_{+3.0}$								
Cross-Section	5	5			10	10	6	30	30
Multijet Norm. (shape)			2.5						
Mistag (S)				$^{+36.7}_{-30}$					

CDF: loose double-tag (LDT) $WH, ZH \to \not\!\!E_T b\bar{b}$ channel relative uncertainties (%)

Contribution	ZH	WH	Multijet	Mistags	Top Pair	S. Top	Di-boson	W + HF	Z + HF
Luminosity	3.8	3.8			3.8	3.8	3.8	3.8	3.8
Lumi Monitor	4.4	4.4			4.4	4.4	4.4	4.4	4.4
Tagging SF	8.3	8.3			8.3	8.3	8.3	8.3	8.3
Trigger Eff. (S)	1.2	1.7	1.6		0.9	1.8	2.0	2.5	1.9
Lepton Veto	2.0	2.0			2.0	2.0	2.0	2.0	2.0
PDF Acceptance	3.0	3.0			3.0	3.0	3.0	3.0	3.0
JES (S)	$^{+1.9}_{-1.9}$	$^{+2.4}_{-2.4}$			$^{+3.0}_{-2.8}$	$^{-0.6}_{0.2}$	$^{+4.2}_{-4.2}$	$^{+6.8}_{-5.9}$	$^{+8.3}_{-3.1}$
ISR/FSR	$^{+2.4}_{-2.4}$								
Cross-Section	5.0	5.0			10	10	6	30	30
Multijet Norm.			1.6						
Mistag (S)				$^{+65.2}_{-38.5}$					

CDF: single-tag (ST) $WH, ZH \to \not\!\!E_T b\bar{b}$ channel relative uncertainties (%)

Contribution	ZH	WH	Multijet	Mistags	Top Pair	S. Top	Di-boson	W + HF	Z + HF
Luminosity	3.8	3.8			3.8	3.8	3.8	3.8	3.8
Lumi Monitor	4.4	4.4			4.4	4.4	4.4	4.4	4.4
Tagging SF	5.2	5.2			5.2	5.2	5.2	5.2	5.2
Trigger Eff. (S)	1.2	1.7	1.6		0.9	1.8	2.0	2.5	1.9
Lepton Veto	2.0	2.0			2.0	2.0	2.0	2.0	2.0
PDF Acceptance	3.0	3.0			3.0	3.0	3.0	3.0	3.0
JES (S)	$^{+2.6}_{-2.6}$	$^{+3.3}_{-3.1}$			$^{-0.8}_{+0.6}$	$^{+2.7}_{-2.8}$	$^{+5.1}_{-5.1}$	$^{+8.2}_{-6.8}$	$^{+10.8}_{-3.4}$
ISR/FSR	$^{+2.0}_{-2.0}$								
Cross-Section	5.0	5.0			10	10	6	30	30
Multijet Norm.			0.7						
Mistag (S)				$^{+17.9}_{-17.4}$					

TABLE XIII: Systematic uncertainties on the signal and background contributions for D0's $ZH \rightarrow \nu\nu b\bar{b}$ loose single tag (LST) and double tag (LDT) channels. Systematic uncertainties are listed by name; see the original references for a detailed explanation of their meaning and on how they are derived. Systematic uncertainties for VH (WH+ZH) shown in this table are obtained for $m_H = 115$ GeV/c^2. Uncertainties are relative, in percent, and are symmetric unless otherwise indicated. Shape uncertainties are labeled with an "S", and "SH" represents a shape only uncertainty.

D0: single tag (LST) $ZH \rightarrow \nu\nu b\bar{b}$ channel relative uncertainties (%)

Contribution	Top	V+HF	V+LF	Diboson	Total Bkgd	VH
Jet ID/Reco Eff (S)	2.0	2.0	2.0	2.0	1.9	2.0
Jet Energy Scale (S)	2.2	1.6	3.1	1.0	2.5	0.5
Jet Resolution (S)	0.5	0.3	0.3	0.9	0.3	0.8
Vertex Conf. / Taggability (S)	3.2	1.9	1.7	1.8	1.7	1.6
b Tagging (S)	1.1	0.8	1.8	1.2	1.3	3.2
Lepton Identification	1.6	0.9	0.8	1.0	0.8	1.1
Trigger	2.0	2.0	2.0	2.0	1.9	2.0
Heavy Flavor Fractions	–	20.0	–	–	4.1	–
Cross Sections	10.0	10.2	10.2	7.0	9.8	6.0
Signal Branching Fractions	–	–	–	–	–	1-9
Luminosity	6.1	6.1	6.1	6.1	5.8	6.1
Multijet Normalization	–	–	–	–	1.3	–
ALPGEN MLM (S)	–	–	SH	–	–	–
ALPGEN Scale (S)	–	SH	SH	–	–	–
Underlying Event (S)	–	SH	SH	–	–	–
PDF, reweighting (S)	SH	SH	SH	SH	SH	SH
Total uncertainty	12.8	23.6	12.9	10.1	12.3	9.8

D0: double tag (LDT) $ZH \rightarrow \nu\nu b\bar{b}$ channel relative uncertainties (%)

Contribution	Top	V+HF	V+LF	Diboson	Total Bkgd	VH
Jet ID/Reco Eff	2.0	2.0	2.0	2.0	1.9	2.0
Jet Energy Scale	2.1	1.6	3.4	1.2	2.2	0.2
Jet Resolution	0.7	0.4	0.5	1.5	0.5	0.7
Vertex Conf. / Taggability	2.6	1.6	1.6	1.8	1.7	1.4
b Tagging	6.2	4.3	4.3	3.7	3.6	5.8
Lepton Identification	2.0	0.9	0.8	0.9	1.0	1.1
Trigger	2.0	2.0	2.0	2.0	1.9	2.0
Heavy Flavor Fractions	–	20.0	–	–	8.0	–
Cross Sections	10.0	10.2	10.2	7.0	9.8	6.0
Signal Branching Fractions	–	–	–	–	–	1-9
Luminosity	6.1	6.1	6.1	6.1	5.8	6.1
Multijet Normalilzation	–	–	–	–	1.0	–
ALPGEN MLM pos/neg(S)	–	–	SH	–	–	–
ALPGEN Scale (S)	–	SH	SH	–	–	–
Underlying Event (S)	–	SH	SH	–	–	–
PDF, reweighting (S)	SH	SH	SH	SH	SH	SH
Total uncertainty	14.1	24.0	13.5	10.7	13.9	10.9

TABLE XIV: Systematic uncertainties on the signal and background contributions for CDF's $ZH \to \mu^+\mu^- b\bar{b}$ single tag (ST), tight double tag (TDT), and loose double tag (LDT) channels. Systematic uncertainties are listed by name; see the original references for a detailed explanation of their meaning and on how they are derived. Systematic uncertainties for ZH shown in this table are obtained for $m_H = 115$ GeV/c^2. Uncertainties are relative, in percent, and are symmetric unless otherwise indicated. Shape uncertainties are labeled with an "S".

CDF: single tag (ST) $ZH \to \mu^+\mu^- b\bar{b}$ channel relative uncertainties (%)

Contribution	Fakes	$t\bar{t}$	WW	WZ	ZZ	$Z + b\bar{b}$	$Z + c\bar{c}$	Mistags	ZH
Luminosity ($\sigma_{\text{inel}}(p\bar{p})$)		3.8	3.8	3.8	3.8	3.8	3.8		3.8
Luminosity Monitor		4.4	4.4	4.4	4.4	4.4	4.4		4.4
Lepton ID		1	1	1	1	1	1		1
Lepton Energy Scale		1.5	1.5	1.5	1.5	1.5	1.5		1.5
Fake Leptons	5								
Mistag Rate								$^{+13.6}_{-13.7}$	
Jet Energy Scale (S)		$^{+1.8}_{-1.9}$	$^{+18.7}_{-3.7}$	$^{+3.9}_{-4.3}$	$^{+4.3}_{-5.4}$	$^{+7.9}_{-6.7}$	$^{+7.9}_{-6.6}$		$^{+1.7}_{-2.6}$
b-tag Rate		5.2	5.2	5.2	5.2	5.2	5.2		5.2
$t\bar{t}$ Cross Section		10							
Diboson Cross Section			6	6	6				
Z+HF Cross Section						40	40		
ZH Cross Section									5
ISR/FSR									1
NN Trigger Model		5	5	5	5	5	5		5

CDF: tight double tag (TDT) $ZH \to \mu^+\mu^- b\bar{b}$ channel relative uncertainties (%)

Contribution	Fakes	$t\bar{t}$	WZ	ZZ	WW	$Z + b\bar{b}$	$Z + c\bar{c}$	Mistags	ZH
Luminosity ($\sigma_{\text{inel}}(p\bar{p})$)		3.8	3.8	3.8	3.8	3.8	3.8		3.8
Luminosity Monitor		4.4	4.4	4.4	4.4	4.4	4.4		4.4
Lepton ID		1	1	1	1	1	1		1
Lepton Energy Scale		1.5	1.5	1.5	1.5	1.5	1.5		1.5
Fake Leptons	5								
Mistag Rate								$^{+28.7}_{-25.1}$	
Jet Energy Scale (S)		$^{+1.6}_{-1.7}$	$^{+3.5}_{-3.7}$	$^{+3.5}_{-3.7}$	$^{+4.1}_{-4.4}$	$^{+7.5}_{-3.8}$	$^{+6.6}_{-5.2}$		$^{+1.4}_{-2.3}$
b-tag Rate		10.2	10.2	10.2	10.2	10.2	10.2		10.2
$t\bar{t}$ Cross Section		10							
Diboson Cross Section			6	6	6				
Z+HF Cross Section						40	40		
ZH Cross Section									5
ISR/FSR									5
NN Trigger Model		5	5	5	5	5	5		5

CDF: loose double tag (LDT) $ZH \to \mu^+\mu^- b\bar{b}$ channel relative uncertainties (%)

Contribution	Fakes	$t\bar{t}$	WW	WZ	ZZ	$Z + b\bar{b}$	$Z + c\bar{c}$	Mistags	ZH
Luminosity ($\sigma_{\rm inel}(p\bar{p})$)		3.8	3.8	3.8	3.8	3.8	3.8		3.8
Luminosity Monitor		4.4	4.4	4.4	4.4	4.4	4.4		4.4
Lepton ID		1	1	1	1	1	1		1
Lepton Energy Scale		1.5	1.5	1.5	1.5	1.5	1.5		1.5
Fake Leptons	5								
Mistag Rate								$^{+27.2}_{-24.0}$	
Jet Energy Scale (S)		$^{+1.6}_{-1.8}$	$^{+3.5}_{-3.7}$	$^{+4.6}_{-7.6}$	$^{+4.0}_{-4.2}$	$^{+6.9}_{-5.9}$	$^{+7.8}_{-5.9}$		$^{+1.5}_{-2.4}$
b-tag Rate		8.7	8.7	8.7	8.7	8.7	8.7		8.7
$t\bar{t}$ Cross Section		10							
Diboson Cross Section			6	6	6				
Z+HF Cross Section						40	40		
ZH Cross Section									5
ISR/FSR									2
NN Trigger Model		5	5	5	5	5	5		5

TABLE XV: Systematic uncertainties on the signal and background contributions for CDF's $ZH \to e^+e^- b\bar{b}$ single tag (ST), tight double tag (TDT), and loose double tag (LDT) channels. Systematic uncertainties are listed by name; see the original references for a detailed explanation of their meaning and on how they are derived. Systematic uncertainties for ZH shown in this table are obtained for $m_H = 115$ GeV/c^2. Uncertainties are relative, in percent, and are symmetric unless otherwise indicated. Shape uncertainties are labeled with an "S".

CDF: single tag (ST) $ZH \to e^+e^- b\bar{b}$ channel relative uncertainties (%)

Contribution	Fakes	Top	WW	WZ	ZZ	$Z + b\bar{b}$	$Z + c\bar{c}$	Z+LF	ZH
Luminosity ($\sigma_{\rm inel}(p\bar{p})$)	0	3.8	3.8	3.8	3.8	3.8	3.8	0	3.8
Luminosity Monitor	0	4.4	4.4	4.4	4.4	4.4	4.4	0	4.4
Trigger Emulation	0	1	1	1	1	1	1	0	1
Lepton ID	0	2	2	2	2	2	2	0	2
Lepton Energy Scale	0	3	3	3	3	3	3	0	3
ZH Cross Section	0	0	0	0	0	0	0	0	5
Fake Leptons	50	0	0	0	0	0	0	0	0
B-Tag Efficiency	0	5.2	5.2	5.2	5.2	5.2	5.2	0	5.2
$t\bar{t}$ Cross Section	0	10	0	0	0	0	0	0	0
Diboson Cross Section	0	0	6	6	6	0	0	0	0
$\sigma(p\bar{p} \to Z + HF)$	0	0	0	0	40	40	40	0	0
ISR/FSR	0	0	0	0	0	0	0	0	4.0
Mistag Rate (S)	0	0	0	0	0	0	0	$^{+13.9}_{-13.8}$	0
Jet Energy Scale (S)	0	$^{+1.9}_{-2.5}$	$^{+19.6}_{-4.0}$	$^{+5.2}_{-6.2}$	$^{+5.3}_{-7.1}$	$^{+12.1}_{-11.1}$	$^{+4.1}_{-9.9}$	0	$^{+3.0}_{-4.3}$

CDF: tight double tag (TDT) $ZH \to e^+e^-b\bar{b}$ channel relative uncertainties (%)

Contribution	Fakes	Top	WZ	ZZ	$Z+b\bar{b}$	$Z+c\bar{c}$	Z+LF	ZH
Luminosity ($\sigma_{\rm inel}(p\bar{p})$)	0	3.8	3.8	3.8	3.8	3.8	0	3.8
Luminosity Monitor	0	4.4	4.4	4.4	4.4	4.4	0	4.4
Trigger Emulation	0	1	1	1	1	1	0	1
Lepton ID	0	2	2	2	2	2	0	2
Lepton Energy Scale	0	3	3	3	3	3	0	3
ZH Cross Section	0	0	0	0	0	0	0	5
Fake Leptons	50	0	0	0	0	0	0	0
B-Tag Efficiency	0	10.4	10.4	10.4	10.4	10.4	0	10.4
$t\bar{t}$ Cross Section	0	10	0	0	0	0	0	0
Diboson Cross Section	0	0	6	6	0	0	0	0
$\sigma(p\bar{p} \to Z+HF)$	0	0	0	40	40	40	0	0
ISR/FSR	0	0	0	0	0	0	0	4.0
Mistag Rate (S)	0	0	0	0	0	0	$^{+29.3}_{-25.4}$	0
Jet Energy Scale (S)	0	$^{+1.4}_{-2.6}$	$^{+7.8}_{-3.1}$	$^{+3.4}_{-5.9}$	$^{+6.8}_{-6.6}$	$^{+1.0}_{-3.7}$	0	$^{+1.6}_{-2.7}$

CDF: loose double tag (LDT) $ZH \to e^+e^-b\bar{b}$ channel relative uncertainties (%)

Contribution	Fakes	Top	WW	WZ	ZZ	$Z+b\bar{b}$	$Z+c\bar{c}$	Z+LF	ZH
Luminosity ($\sigma_{\rm inel}(p\bar{p})$)	0	3.8	3.8	3.8	3.8	3.8	3.8	0	3.8
Luminosity Monitor	0	4.4	4.4	4.4	4.4	4.4	4.4	0	4.4
Trigger Emulation	0	1	1	1	1	1	1	0	1
Lepton ID	0	2	2	2	2	2	2	0	2
Lepton Energy Scale	0	3	3	3	3	3	3	0	3
ZH Cross Section	0	0	0	0	0	0	0	0	5
Fake Leptons	50	0	0	0	0	0	0	0	0
B-Tag Efficiency	0	8.7	8.7	8.7	8.7	8.7	8.7	0	8.7
$t\bar{t}$ Cross Section	0	10	0	0	0	0	0	0	0
Diboson Cross Section	0	0	6	6	6	0	0	0	0
$\sigma(p\bar{p} \to Z+HF)$	0	0	0	0	40	40	40	0	0
ISR/FSR	0	0	0	0	0	0	0	0	4.0
Mistag Rate (S)	0	0	0	0	0	0	0	$^{+25.5}_{-21.4}$	0
Jet Energy Scale (S)	0	$^{+1.3}_{-2.3}$	0	$^{+7.5}_{-0.1}$	$^{+4.1}_{-4.4}$	$^{+8.2}_{-7.8}$	$^{+3.3}_{-5.5}$	0	$^{+2.1}_{-2.7}$

TABLE XVI: Systematic uncertainties on the contributions for D0's $ZH \to \ell^+\ell^- b\bar{b}$ channels. Systematic uncertainties are listed by name; see the original references for a detailed explanation of their meaning and on how they are derived. Systematic uncertainties for ZH shown in this table are obtained for $m_H = 115$ GeV/c^2. Uncertainties are relative, in percent, and are symmetric unless otherwise indicated. Shape uncertainties are labeled with an "S".

D0: $ZH \to \ell\ell b\bar{b}$ analyses relative uncertainties (%)

Contribution	Signal	Multijet	Z+LF	$Zb\bar{b}$	$Zc\bar{c}$	Diboson	$t\bar{t}$
hline Jet Energy Scale (S)	1.5		3.0	8.4	10	3.3	1.5
Jet Energy Resolution (S)	0.3		3.9	5.2	5.3	0.04	0.6
Jet ID (S)	0.6		0.9	0.6	0.2	1.0	0.3
Taggability (S)	5.1		5.2	7.2	7.3	6.9	6.5
Zp_T Model (S)			2.7	1.4	1.5		
HF Tagging Efficiency (S)	4.9			5.0	9.4		5.2
LF Tagging Efficiency (S)			73			5.8	
ee Multijet Shape (S)		53					
Multijet Normalization		20-50					
Z+jets Jet Angles (S)			1.7	2.7	2.8		
Alpgen MLM (S)			0.3				
Alpgen Scale (S)			0.4	0.2	0.2		
Underlying Event (S)			0.2	0.05	0.08		
Trigger (S)	0.4		0.03	0.2	0.3	0.3	0.4
Cross Sections	6.2			20	20	7	10
Signal Branching Fraction	1-9						
Normalization	8		1.3	1.3	1.3	8	8
PDFs	0.55		1	2.4	1.1	0.66	5.9

D0: Double Tag (DT) $ZH \to \ell\ell b\bar{b}$ analysis relative uncertainties (%)

Contribution	Signal	Multijet	Z+LF	$Zb\bar{b}$	$Zc\bar{c}$	Diboson	$t\bar{t}$
Jet Energy Scale (S)	2.3		4.0	6.4	8.2	3.8	2.7
Jet Energy Resolution(S)	0.6		2.6	3.9	4.1	0.9	1.5
JET ID (S)	0.8		0.7	0.3	0.2	0.7	0.4
Taggability (S)	3.6		8.6	6.5	8.2	4.6	2.1
Z_{p_T} Model (S)			1.6	1.3	1.4		
HF Tagging Efficiency (S)	0.8			1.3	3.2		0.7
LF Tagging Efficiency (S)			72			4.0	
ee Multijet Shape (S)		59					
Multijet Normalization		20-50					
Z+jets Jet Angles (S)			2.0	1.5	1.5		
Alpgen MLM (S)			0.4				
Alpgen Scale (S)			0.2	0.2	0.2		
Underlying Event(S)			0.07	0.02	0.1		
Trigger (S)	0.4		0.3	0.2	0.1	0.2	0.5
Cross Sections	6.2			20	20	7	10
Signal Branching Fraction	1-9						
Normalization	8		1.3	1.3	1.3	8	8
PDFs	0.55		1	2.4	1.1	0.66	5.9

TABLE XVII: Systematic uncertainties on the signal and background contributions for CDF's $H \to W^+W^- \to \ell^\pm\ell'^\mp$ channels with zero, one, and two or more associated jets. These channels are sensitive to gluon fusion production (all channels) and WH, ZH and VBF production. Systematic uncertainties are listed by name (see the original references for a detailed explanation of their meaning and on how they are derived). Systematic uncertainties for H shown in this table are obtained for $m_H = 160$ GeV/c^2. Uncertainties are relative, in percent, and are symmetric unless otherwise indicated. The uncertainties associated with the different background and signal processed are correlated within individual jet categories unless otherwise noted. Boldface and italics indicate groups of uncertainties which are correlated with each other but not the others on the line.

CDF: $H \to W^+W^- \to \ell^\pm\ell'^\mp$ with no associated jet channel relative uncertainties (%)

Contribution	WW	WZ	ZZ	$t\bar{t}$	DY	$W\gamma$	W+jet	$gg \to H$	WH	ZH	VBF
Cross Section :											
Scale (Inclusive)								13.4			
Scale (1+ Jets)								-23.0			
Scale (2+ Jets)								0.0			
PDF Model								7.6			
Total	*6.0*	*6.0*	*6.0*	7.0					**5.0**	**5.0**	10.0
Acceptance :											
Scale (jets)	*0.3*										
PDF Model (leptons)								2.7			
PDF Model (jets)	*1.1*							5.5			
Higher-order Diagrams		*10.0*	*10.0*	10.0		10.0			**10.0**	**10.0**	**10.0**
$\not\!\!E_T$ Modeling					19.5						
Conversion Modeling						10.0					
Jet Fake Rates											
(Low S/B)							22.0				
(High S/B)							26.0				
Jet Energy Scale	*2.6*	*6.1*	*3.4*	*26.0*	*17.5*	*3.1*		*5.0*	*10.5*	*5.0*	*11.5*
Lepton ID Efficiencies	*3.8*	*3.8*	*3.8*	*3.8*	*3.8*			*3.8*	*3.8*	*3.8*	*3.8*
Trigger Efficiencies	*2.0*	*2.0*	*2.0*	*2.0*	*2.0*			*2.0*	*2.0*	*2.0*	*2.0*
Luminosity	*3.8*	*3.8*	*3.8*	*3.8*	*3.8*			*3.8*	*3.8*	*3.8*	*3.8*
Luminosity Monitor	*4.4*	*4.4*	*4.4*	*4.4*	*4.4*			*4.4*	*4.4*	*4.4*	*4.4*

CDF: $H \to W^+W^- \to \ell^\pm\ell'^\mp$ with one associated jet channel relative uncertainties (%)

Contribution	WW	WZ	ZZ	$t\bar{t}$	DY	$W\gamma$	W+jet	$gg \to H$	WH	ZH	VBF
Cross Section :											
Scale (Inclusive)								0.0			
Scale (1+ Jets)								35.0			
Scale (2+ Jets)								-12.7			
PDF Model								17.3			
Total	*6.0*	*6.0*	*6.0*	7.0					**5.0**	**5.0**	10.0
Acceptance :											
Scale (jets)	*-4.0*										
PDF Model (leptons)								*3.6*			
PDF Model (jets)	*4.7*							-6.3			
Higher-order Diagrams		*10.0*	*10.0*	10.0		10.0			**10.0**	**10.0**	**10.0**
$\not\!\!E_T$ Modeling					20.0						
Conversion Modeling						10.0					
Jet Fake Rates											
(Low S/B)							23.0				
(High S/B)							29.0				
Jet Energy Scale	*-5.5*	*-1.0*	*-4.3*	*-13.0*	*-6.5*	*-9.5*		*-4.0*	*-8.5*	*-7.0*	*-6.5*
Lepton ID Efficiencies	*3.8*	*3.8*	*3.8*	*3.8*	*3.8*			*3.8*	*3.8*	*3.8*	*3.8*
Trigger Efficiencies	*2.0*	*2.0*	*2.0*	*2.0*	*2.0*			*2.0*	*2.0*	*2.0*	*2.0*
Luminosity	*3.8*	*3.8*	*3.8*	*3.8*	*3.8*			*3.8*	*3.8*	*3.8*	*3.8*
Luminosity Monitor	*4.4*	*4.4*	*4.4*	*4.4*	*4.4*			*4.4*	*4.4*	*4.4*	*4.4*

CDF: $H \to W^+W^- \to \ell^\pm\ell'^\mp$ with two or more associated jets channel relative uncertainties (%)

Contribution	WW	WZ	ZZ	$t\bar{t}$	DY	$W\gamma$	W+jet	$gg \to H$	WH	ZH	VBF
Cross Section :											
Scale (Inclusive)								0.0			
Scale (1+ Jets)								0.0			
Scale (2+ Jets)								33.0			
PDF Model								29.7			
Total	*6.0*	*6.0*	*6.0*	7.0					**5.0**	**5.0**	10.0
Acceptance :											
Scale (jets)	*-8.2*										
PDF Model (leptons)								*4.8*			
PDF Model (jets)	*4.2*							-12.3			
Higher-order Diagrams		*10.0*	*10.0*	10.0		10.0			**10.0**	**10.0**	**10.0**
$\not\!\!E_T$ Modeling					25.5						
Conversion Modeling						10.0					
Jet Fake Rates							28.0				
Jet Energy Scale	*-14.8*	*-12.9*	*-12.1*	*-1.7*	*-29.2*	*-22.0*		*-17.0*	*-4.0*	*-2.3*	*-4.0*
b-tag Veto				3.8							
Lepton ID Efficiencies	*3.8*	*3.8*	*3.8*	*3.8*	*3.8*			*3.8*	*3.8*	*3.8*	*3.8*
Trigger Efficiencies	*2.0*	*2.0*	*2.0*	*2.0*	*2.0*			*2.0*	*2.0*	*2.0*	*2.0*
Luminosity	*3.8*	*3.8*	*3.8*	*3.8*	*3.8*			*3.8*	*3.8*	*3.8*	*3.8*
Luminosity Monitor	*4.4*	*4.4*	*4.4*	*4.4*	*4.4*			*4.4*	*4.4*	*4.4*	*4.4*

TABLE XVIII: Systematic uncertainties on the signal and background contributions for CDF's low-$M_{\ell\ell}$ $H \to W^+W^- \to \ell^\pm\ell'^\mp$ channel with zero or one associated jets. This channel is sensitive to only gluon fusion production. Systematic uncertainties are listed by name (see the original references for a detailed explanation of their meaning and on how they are derived). Systematic uncertainties for H shown in this table are obtained for $m_H = 160$ GeV/c^2. Uncertainties are relative, in percent, and are symmetric unless otherwise indicated. The uncertainties associated with the different background and signal processed are correlated within individual categories unless otherwise noted. In these special cases, the correlated uncertainties are shown in either italics or bold face text.

CDF: low $M_{\ell\ell}$ $H \to W^+W^- \to \ell^\pm\ell'^\mp$ with zero or one associated jets channel relative uncertainties (%)

Contribution	WW	WZ	ZZ	$t\bar{t}$	DY	$W\gamma$	W+jet(s)	$gg \to H$	WH	ZH	VBF
Cross Section :											
Scale (Inclusive)								8.1			
Scale (1+ Jets)								0.0			
Scale (2+ Jets)								-5.1			
PDF Model								10.5			
Total	*6.0*	*6.0*	*6.0*	7.0	5.0				**5.0**	**5.0**	10.0
Acceptance :											
Scale (jets)	*-0.4*										
PDF Model (leptons)								*1.0*			
PDF Model (jets)	*1.6*							2.1			
Higher-order Diagrams		*10.0*	*10.0*	10.0	10.0				**10.0**	**10.0**	**10.0**
Jet Energy Scale	*1.1*	*2.2*	*2.0*	*13.5*	*6.4*	*1.3*		*2.4*	*9.2*	*6.5*	*7.8*
Conversion Modeling						10.0					
Boson Radiation Model					25.0						
Jet Fake Rates							13.5				
Lepton ID Efficiencies	*3.8*	*3.8*	*3.8*	*3.8*	*3.8*			*3.8*	*3.8*	*3.8*	*3.8*
Trigger Efficiencies	*2.0*	*2.0*	*2.0*	*2.0*	*2.0*			*2.0*	*2.0*	*2.0*	*2.0*
Luminosity	*3.8*	*3.8*	*3.8*	*3.8*	*3.8*			*3.8*	*3.8*	*3.8*	*3.8*
Luminosity Monitor	*4.4*	*4.4*	*4.4*	*4.4*	*4.4*			*4.4*	*4.4*	*4.4*	*4.4*

TABLE XIX: Systematic uncertainties on the signal and background contributions for CDF's $H \to W^+W^- \to e^\pm\tau^\mp$ and $H \to W^+W^- \to \mu^\pm\tau^\mp$ channels. These channels are sensitive to gluon fusion production, WH, ZH and VBF production. Systematic uncertainties are listed by name (see the original references for a detailed explanation of their meaning and on how they are derived). Systematic uncertainties for H shown in this table are obtained for $m_H = 160$ GeV/c^2. Uncertainties are relative, in percent, and are symmetric unless otherwise indicated. The uncertainties associated with the different background and signal processed are correlated within individual categories unless otherwise noted. In these special cases, the correlated uncertainties are shown in either italics or bold face text.

CDF: $H \to W^+W^- \to e^\pm\tau^\mp$ channel relative uncertainties ( )

Contribution	WW	WZ	ZZ	$t\bar{t}$	$Z \to \tau\tau$	$Z \to \ell\ell$	W+jet	$W\gamma$	$gg \to H$	WH	ZH	VBF
Cross section	6.0	6.0	6.0	10.0	5.0	5.0			10.3	5	5	10
Measured W cross-section							12					
PDF Model	1.6	2.3	3.2	2.3	2.7	4.6	2.2	3.1	2.5	2.0	1.9	1.8
Higher order diagrams	10	10	10	10	10	10		10		10	10	10
Conversion modeling								10				
Trigger Efficiency	0.5	0.6	0.6	0.6	0.7	0.5	0.6	0.6	0.5	0.5	0.6	0.5
Lepton ID Efficiency	0.4	0.5	0.5	0.4	0.4	0.4	0.5	0.4	0.4	0.4	0.4	0.4
τ ID Efficiency	1.0	1.3	1.9	1.3	2.1			0.3	2.8	1.6	1.7	2.8
Jet into τ Fake rate	5.8	4.8	2.0	5.1		0.1	8.8			4.2	4.0	0.4
Lepton into τ Fake rate	0.2	0.1	0.6	0.2		2.3		2.1	0.15	0.06	0.15	0.11
W+jet scale							1.6					
MC Run dependence	2.6	2.6	2.6				2.6					
Luminosity	3.8	3.8	3.8	3.8	3.8	3.8	3.8	3.8	3.8	3.8	3.8	3.8
Luminosity Monitor	4.4	4.4	4.4	4.4	4.4	4.4	4.4	4.4	4.4	4.4	4.4	4.4

CDF: $H \to W^+W^- \to \mu^\pm\tau^\mp$ channel relative uncertainties (%)

Contribution	WW	WZ	ZZ	$t\bar{t}$	$Z \to \tau\tau$	$Z \to \ell\ell$	W+jet	$W\gamma$	$gg \to H$	WH	ZH	VBF
Cross section	6.0	6.0	6.0	10.0	5.0	5.0			10.4	5	5	10
Measured W cross-section							12					
PDF Model	1.5	2.1	2.9	2.1	2.5	4.3	2.0	2.9	2.6	2.2	2.0	2.2
Higher order diagrams	10	10	10	10				11		10	10	10
Trigger Efficiency	1.3	0.7	0.7	1.1	0.9	1.3	1.0	1.0	1.3	1.3	1.2	1.3
Lepton ID Efficiency	1.1	1.4	1.4	1.1	1.2	1.1	1.4	1.3	1.0	1.0	1.0	1.0
τ ID Efficiency	1.0	1.2	1.4	1.6	1.9				2.9	1.6	1.7	2.8
Jet into τ Fake rate	5.8	5.0	4.4	4.4		0.2	8.8			4.5	4.2	0.4
Lepton into τ Fake rate	0.06	0.05	0.09	0.04		1.9		1.2	0.04	0.02	0.02	0.04
W+jet scale							1.4					
MC Run dependence	3.0	3.0	3.0				3.0					
Luminosity	3.8	3.8	3.8	3.8	3.8	3.8	3.8	3.8	3.8	3.8	3.8	3.8
Luminosity Monitor	4.4	4.4	4.4	4.4	4.4	4.4	4.4	4.4	4.4	4.4	4.4	4.4

TABLE XX: Systematic uncertainties on the signal and background contributions for CDF's $WH \to WWW \to \ell^{\pm}\ell'^{\pm}$ channel with one or more associated jets and $WH \to WWW \to \ell^{\pm}\ell'^{\pm}\ell''^{\mp}$ channel. These channels are sensitive to only WH and ZH production. Systematic uncertainties are listed by name (see the original references for a detailed explanation of their meaning and on how they are derived). Systematic uncertainties for H shown in this table are obtained for $m_H = 160$ GeV/c^2. Uncertainties are relative, in percent, and are symmetric unless otherwise indicated. The uncertainties associated with the different background and signal processed are correlated within individual categories unless otherwise noted. In these special cases, the correlated uncertainties are shown in either italics or bold face text.

CDF: $WH \to WWW \to \ell^{\pm}\ell'^{\pm}$ channel relative uncertainties (%)

Contribution	WW	WZ	ZZ	$t\bar{t}$	DY	$W\gamma$	W+jet	WH	ZH
Cross Section	*6.0*	*6.0*	*6.0*	7.0	5.0			**5.0**	**5.0**
Scale (Acceptance)	*-6.1*								
PDF Model (Acceptance)	*5.7*								
Higher-order Diagrams		*10.0*	*10.0*	10.0	10.0	10.0		**10.0**	**10.0**
Conversion Modeling						10.0			
Jet Fake Rates							38.5		
Jet Energy Scale	*-14.0*	*-3.9*	*-2.8*	*-0.6*	*-7.7*	*-7.6*		*-1.0*	*-0.7*
Charge Mismeasurement Rate	*40.0*				*40.0*				
Lepton ID Efficiencies	*3.8*	*3.8*	*3.8*	*3.8*	*3.8*			*3.8*	*3.8*
Trigger Efficiencies	*2.0*	*2.0*	*2.0*	*2.0*	*2.0*			*2.0*	*2.0*
Luminosity	*3.8*	*3.8*	*3.8*	*3.8*	*3.8*			*3.8*	*3.8*
Luminosity Monitor	*4.4*	*4.4*	*4.4*	*4.4*	*4.4*			*4.4*	*4.4*

CDF: $WH \to WWW \to \ell^{\pm}\ell'^{\pm}\ell''^{\mp}$ channel relative uncertainties (%)

Contribution	WZ	ZZ	$Z\gamma$	$t\bar{t}$	Fakes	WH	ZH
Cross Section	*6.0*	*6.0*	10.0	7.0		**5.0**	**5.0**
Higher-order Diagrams	*10.0*	*10.0*	15.0	10.0		**10.0**	**10.0**
Jet Energy Scale			*-2.7*				
Jet Fake Rates					25.6		
b-Jet Fake Rates				27.3			
MC Run Dependence			5.0				
Lepton ID Efficiencies	*5.0*	*5.0*		*5.0*		*5.0*	*5.0*
Trigger Efficiencies	*2.0*	*2.0*		*2.0*		*2.0*	*2.0*
Luminosity	*3.8*	*3.8*		*3.8*		*3.8*	*3.8*
Luminosity Monitor	*4.4*	*4.4*		*4.4*		*4.4*	*4.4*

TABLE XXI: Systematic uncertainties on the signal and background contributions for CDF's $ZH \to ZWW \to \ell^{\pm}\ell^{\mp}\ell'^{\pm}$ channels with 1 jet and 2 or more jets. These channels are sensitive to only WH and ZH production. Systematic uncertainties are listed by name (see the original references for a detailed explanation of their meaning and on how they are derived). Systematic uncertainties for H shown in this table are obtained for $m_H = 160$ GeV/c^2. Uncertainties are relative, in percent, and are symmetric unless otherwise indicated. The uncertainties associated with the different background and signal processed are correlated within individual categories unless otherwise noted. In these special cases, the correlated uncertainties are shown in either italics or bold face text.

CDF: $ZH \to ZWW \to \ell^{\pm}\ell^{\mp}\ell'^{\pm}$ with one associated jet channel relative uncertainties (%)

Contribution	WZ	ZZ	$Z\gamma$	$t\bar{t}$	Fakes	WH	ZH
Cross Section	*6.0*	*6.0*	10.0	7.0		**5.0**	**5.0**
Higher-order Diagrams	*10.0*	*10.0*	15.0	10.0		**10.0**	**10.0**
Jet Energy Scale	*-7.6*	*-2.3*	*-5.3*	*9.4*		*-9.0*	*8.1*
Jet Fake Rates					24.8		
b-Jet Fake Rates				42.0			
MC Run Dependence			5.0				
Lepton ID Efficiencies	*5.0*	*5.0*		*5.0*		*5.0*	*5.0*
Trigger Efficiencies	*2.0*	*2.0*		*2.0*		*2.0*	*2.0*
Luminosity	*3.8*	*3.8*		*3.8*		*3.8*	*3.8*
Luminosity Monitor	*4.4*	*4.4*		*4.4*		*4.4*	*4.4%*

CDF: $ZH \to ZWW \to \ell^{\pm}\ell^{\mp}\ell'^{\pm}$ with two or more associated jets channel relative uncertainties (%)

Contribution	WZ	ZZ	$Z\gamma$	$t\bar{t}$	Fakes	WH	ZH
Cross Section	*6.0*	*6.0*	10.0	7.0		**5.0**	**5.0**
Higher-order Diagrams	*10.0*	*10.0*	15.0	10.0		**10.0**	**10.0**
Jet Energy Scale	*-17.8*	*-13.1*	*-18.2*	*-3.6*		*-15.4*	*-4.9*
Jet Fake Rates					25.6		
b-Jet Fake Rates				22.2			
MC Run Dependence			5.0				
Lepton ID Efficiencies	*5.0*	*5.0*		*5.0*		*5.0*	*5.0*
Trigger Efficiencies	*2.0*	*2.0*		*2.0*		*2.0*	*2.0*
Luminosity	*3.8*	*3.8*		*3.8*		*3.8*	*3.8*
Luminosity Monitor	*4.4*	*4.4*		*4.4*		*4.4*	*4.4*

TABLE XXII: Systematic uncertainties on the signal and background contributions for D0's $H \to WW \to \ell^{\pm}\ell'^{\mp}$ channels. Systematic uncertainties are listed by name; see the original references for a detailed explanation of their meaning and on how they are derived. Shape uncertainties are labeled with the "S" designation. Systematic uncertainties shown in this table are obtained for the $m_H = 165$ GeV/c^2 Higgs selection. Uncertainties are relative, in percent, and are symmetric unless otherwise indicated.

D0: $H \to WW \to \ell^{\pm}\ell'^{\mp}$ channels relative uncertainties (%)

Contribution	Diboson	$Z/\gamma^* \to \ell\ell$	$W + jet/\gamma$	$t\bar{t}$	Multijet	$gg \to H$	$qq \to qqH$	VH
Luminosity/Normalization	6	6	6	6	20-30	6	6	6
Jet-bin Normalization:	–	2-15	20	–	–	–	–	–
Cross Section (scale/PDF)	7	6	6	10	–	13-33/7.6-30	4.9	6.1
Signal Branching Fraction	–	–	–	–	–	0-7.3	0-7.3	0-7.3
PDF	2.5	2.5	2.5	2.5	–	–	–	–
EM Identification	2.5	2.5	2.5	2.5	–	2.5	2.5	2.5
EM Resolution (each)	2	2	2	2	–	2	2	2
Muon Identification	4	4	4	4	–	4	4	4
Vertex Confirmation (S)	2-6	1-7	1-6	1-8	–	1-8	1-8	1-8
Jet identification (S)	2-5	2-5	2-5	2-5	–	2-5	2-5	2-5
Jet Energy Scale (S)	2-3	1-4	1-8	1-4	–	1-10	1-10	1-10
Jet Energy Resolution(S)	1-4	1-4	1-12	1-3	–	1-12	1-12	1-12
B-tagging	10	10	10	5	–	10	10	10

TABLE XXIII: Systematic uncertainties on the signal and background contributions for D0's $H \to W^+W^- \to \mu\nu\tau_{\rm had}\nu$ channel. Systematic uncertainties are listed by name; see the original references for a detailed explanation of their meaning and on how they are derived. Shape uncertainties are labeled with the shape designation (S). Systematic uncertainties shown in this table are obtained for the $m_H = 165$ GeV/c^2 Higgs selection. Uncertainties are relative, in percent, and are symmetric unless otherwise indicated.

D0: $H \to W^+W^- \to \mu\nu\tau_{\rm had}\nu$ channel relative uncertainties (%)

Contribution	Diboson	$Z/\gamma^* \to \ell\ell$	W+jets	$t\bar{t}$	Multijet	$gg \to H$	$qq \to qqH$	VH
Luminosity ($\sigma_{\rm inel}(p\bar{p})$)	4.6	4.6	-	4.6	-	4.6	4.6	4.6
Luminosity Monitor	4.1	4.1	-	4.1	-	4.1	4.1	4.1
Trigger	5.0	5.0	-	5.0	-	5.0	5.0	5.0
Lepton ID	3.7	3.7	-	3.7	-	3.7	3.7	3.7
EM veto	5.0	-	-	5.0	-	5.0	5.0	5.0
Tau Energy Scale (S)	1.0	1.1	-	<1	-	<1	<1	<1
Jet Energy Scale (S)	8.0	<1	-	1.8	-	2.5	2.5	2.5
Jet identification (S)	<1	<1	-	7.5	-	5.0	5.0	5.0
Multijet (S)	-	-	-	-	20-50	-	-	-
Cross Section (scale/PDF)	7.0	4.0	-	10	-	7/8	4.9	6.1
Signal Branching Fraction	-	-	-	-	-	0-7.3	0-7.3	0-7.3
Modeling	1.0	-	10	-	-	3.0	3.0	3.0

TABLE XXIV: Systematic uncertainties on the signal and background contributions for D0's $WH \to WWW \to \ell'^{\pm}\ell'^{\pm}$ channel. Systematic uncertainties are listed by name; see the original references for a detailed explanation of their meaning and on how they are derived. Shape uncertainties are labeled with the "S" designation. Systematic uncertainties for signal shown in this table are obtained for $m_H = 165$ GeV/c^2. Uncertainties are relative, in percent, and are symmetric unless otherwise indicated.

D0: $VH \to \ell^{\pm}\ell'^{\pm} + X$ Run IIa channel relative uncertainties (%)

Contribution	WZ/ZZ	W+jet	ChargeFlip	Multijet	$VH \to \ell\ell X$
Cross section	7	6	0	0	5
Normalization	4.7	4.7	0	0	4.7
Signal Branching Fraction	-	-	-	-	0-7.3
JetID/JES	2	2	0	0	2
Jet-Lepton Fake	0	17-26	0	0	0
Instrumental (ee)	0	0	30	42	0
Instrumental ($e\mu$	0	0	0	28	0
Instrumental ($\mu\mu$)	0	0	27	42	0
Instrumental Model	-	-	S	S	-

D0: $VH \to \ell^{\pm}\ell'^{\pm} + X$ Run IIb channel relative uncertainties (%)

Contribution	WZ/ZZ	W+jet	ChargeFlip	Multijet	$VH \to \ell\ell X$
Cross section	7	6	0	0	5
Normalization	4.7	4.7	0	0	4.7
Signal Branching Fraction	-	-	-	-	0-7.3
JetID/JES	2	2	0	0	2
Jet-Lepton Fake	0	20-32	0	0	0
Instrumental (ee)	0	0	15	30	0
Instrumental ($e\mu$	0	0	0	18	0
Instrumental ($\mu\mu$)	0	0	11	29	0
Instrumental Model	-	-	S	S	-

TABLE XXV: Systematic uncertainties on the signal and background contributions for D0's $H \to WW^* \to \ell\nu jj$ electron and muon channels. Systematic uncertainties are listed by name; see the original references for a detailed explanation of their meaning and on how they are derived. Signal uncertainties are shown for $m_H = 160$ GeV/c^2 for all channels except for WH, shown for $m_H = 115$ GeV/c^2. Those affecting the shape of the RF discriminant are indicated with "Y." Uncertainties are listed as relative changes in normalization, in percent, except for those also marked by "S," where the overall normalization is constant, and the value given denotes the maximum percentage change from nominal in any region of the distribution.

D0: $H \to WW^* \to \ell\nu jj$ Run II channel relative uncertainties (%)

Contribution	Shape	W+jets	Z+jets	Top	Diboson	$gg \to H$	$qq \to qqH$	WH
Jet energy scale	Y	$\binom{+6.7}{-5.4}^S$	< 0.1	± 0.7	± 3.3	$\binom{+5.7}{-4.0}$	± 1.5	$\binom{+2.7}{-2.3}$
Jet identification	Y	$\pm 6.6^S$	< 0.1	± 0.5	± 3.8	± 1.0	± 1.1	± 1.0
Jet resolution	Y	$\binom{+6.6}{-4.1}^S$	< 0.1	± 0.5	$\binom{+1.0}{-0.5}$	$\binom{+3.0}{-0.5}$	± 0.8	± 1.0
Association of jets with PV	Y	$\pm 3.2^S$	$\pm 1.3^S$	± 1.2	± 3.2	± 2.9	± 2.4	$\binom{+0.9}{-0.2}$
Luminosity	N	n/a	n/a	± 6.1	± 6.1	± 6.1	± 6.1	± 6.1
Muon trigger	Y	$\pm 0.4^S$	< 0.1	< 0.1	< 0.1	< 0.1	< 0.1	< 0.1
Electron identification	N	± 4.0	± 4.0	± 4.0	± 4.0	± 4.0	± 4.0	± 4.0
Muon identification	N	± 4.0	± 4.0	± 4.0	± 4.0	± 4.0	± 4.0	± 4.0
ALPGEN tuning	Y	$\pm 1.1^S$	$\pm 0.3^S$	n/a	n/a	n/a	n/a	n/a
Cross Section	N	± 6	± 6	± 10	± 7	± 10	± 10	± 6
Heavy-flavor fraction	Y	± 20	± 20	n/a	n/a	n/a	n/a	n/a
Signal Branching Fraction	N	n/a	n/a	n/a	n/a	0-7.3	0-7.3	0-7.3
PDF	Y	$\pm 2.0^S$	$\pm 0.7^S$	$< 0.1^S$	$< 0.1^S$	$< 0.1^S$	$< 0.1^S$	$< 0.1^S$
		Electron channel				Muon channel		
Multijet Background	Y	± 6.5				± 26		

TABLE XXVI: Systematic uncertainties on the signal and background contributions for CDF's $H \to \ell^{\pm}\ell^{\mp}\ell'^{\pm}\ell'^{\mp}$ channel. This channel is sensitive to gluon fusion production and WH, ZH and VBF production. Systematic uncertainties are listed by name (see the original references for a detailed explanation of their meaning and on how they are derived). Uncertainties are relative, in percent, and are symmetric unless otherwise indicated. The uncertainties associated with the different background and signal processed are correlated unless otherwise noted. Boldface and italics indicate groups of uncertainties which are correlated with each other but not the others on the line.

CDF: $H \to \ell^{\pm}\ell^{\mp}\ell'^{\pm}\ell'^{\mp}$ channel relative uncertainties (%)

Contribution	ZZ	$Z(/\gamma^*)$+jets	$gg \to H$	WH	ZH	VBF
Cross Section :						
Scale			7.0			
PDF Model			7.7			
Total	*10.0*			**5.0**	**5.0**	10.0
$\mathcal{BR}(H \to VV)$			3.0	3.0	3.0	3.0
Acceptance :						
PDF Model	2.7					
Higher-order Diagrams	2.5					
Jet Fake Rates		50.0				
Lepton ID Efficiencies	*3.6*		*3.6*	*3.6*	*3.6*	*3.6*
Trigger Efficiencies	*0.4*		*0.4*	*0.4*	*0.4*	*0.4*
Luminosity	*3.8*		*3.8*	*3.8*	*3.8*	*3.8*
Luminosity Monitor	*4.4*		*4.4*	*4.4*	*4.4*	*4.4*

TABLE XXVII: Systematic uncertainties on the signal and background contributions for CDF's $t\bar{t}H \rightarrow \ell$+jets channels. Systematic uncertainties are listed by name; see the original references for a detailed explanation of their meaning and on how they are derived. Systematic uncertainties for $t\bar{t}H$ shown in this table are obtained for $m_H = 115$ GeV/c^2. Uncertainties are relative, in percent, and are symmetric unless otherwise indicated.

CDF: $t\bar{t}H$ $\ell + \not\!\!E_T$+4 jets relative uncertainties (%)

	1 tight, 1 loose		1 tight, $\geq$ 2 loose		2 tight, 0 loose		2 tight, $\geq$ 1 loose		$\geq$ 3 tight, $\geq$ 0 loose	
Contribution	$t\bar{t}$	$t\bar{t}H$	$t\bar{t}$	$t\bar{t}H$	$t\bar{t}$	$t\bar{t}H$	$t\bar{t}$	$t\bar{t}H$	$t\bar{t}$	$t\bar{t}H$
$t\bar{t}$ Cross Section		10		10		10		10		10
$t\bar{t}H$ Cross Section	10		10		10		10		10	
Luminosity ($\sigma_{\text{inel}}(p\bar{p})$)	3.8	3.8	3.8	3.8	3.8	3.8	3.8	3.8	3.8	3.8
Luminosity Monitor	4.4	4.4	4.4	4.4	4.4	4.4	4.4	4.4	4.4	4.4
B-Tag Efficiency	$^{+1.4}_{-2.5}$	$^{-2.9}_{-2.0}$	$^{+3.3}_{-1.5}$	$^{+0.3}_{+0.3}$	$^{+7.3}_{-9.4}$	$^{+6.7}_{-2.0}$	$^{+8.3}_{-8.8}$	$^{+7.0}_{-7.7}$	$^{+11}_{-12}$	$^{+11}_{-16}$
Mistag Rate	$^{+1.7}_{-2.0}$	$^{-0.4}_{-1.5}$	$^{+10}_{-11}$	$^{-1.1}_{-5.7}$	$^{-1.2}_{+2.7}$	$^{+2.7}_{+3.7}$	$^{+7.6}_{-7.4}$	$^{+1.7}_{+2.4}$	$^{+3.3}_{-5.1}$	$^{+1.6}_{+0.2}$
Jet Energy Scale	$^{+3.8}_{-5.1}$	$^{-13}_{+6.7}$	$^{+2.5}_{-4.5}$	$^{0.0}_{0.0}$	$^{+4.2}_{-4.8}$	$^{-5.9}_{+5.9}$	$^{+2.5}_{-3.8}$	$^{-12}_{0.0}$	$^{+3.3}_{-4.4}$	$^{-12}_{0.0}$
ISR+FSR+PDF	$^{-1.8}_{-1.0}$	$^{-0.1}_{+0.1}$	$^{-1.3}_{+2.3}$	$^{-0.5}_{+0.5}$	$^{-3.8}_{-1.3}$	$^{+0.2}_{-0.2}$	$^{-4.4}_{-1.1}$	$^{+0.0}_{-0.0}$	$^{-2.9}_{-3.5}$	$^{-0.2}_{+0.2}$

CDF: $t\bar{t}H$ $\ell + \not\!\!E_T$+5 jets relative uncertainties (%)

	1 tight, 1 loose		1 tight, $\geq$ 2 loose		2 tight, 0 loose		2 tight, $\geq$ 1 loose		$\geq$ 3 tight, $\geq$ 0 loose	
Contribution	$t\bar{t}$	$t\bar{t}H$	$t\bar{t}$	$t\bar{t}H$	$t\bar{t}$	$t\bar{t}H$	$t\bar{t}$	$t\bar{t}H$	$t\bar{t}$	$t\bar{t}H$
$t\bar{t}$ Cross Section		10		10		10		10		10
$t\bar{t}H$ Cross Section	10		10		10		10		10	
Luminosity ($\sigma_{\text{inel}}(p\bar{p})$)	3.8	3.8	3.8	3.8	3.8	3.8	3.8	3.8	3.8	3.8
Luminosity Monitor	4.4	4.4	4.4	4.4	4.4	4.4	4.4	4.4	4.4	4.4
B-Tag Efficiency	$^{+1.8}_{-3.5}$	$^{-0.4}_{+2.7}$	$^{+4.5}_{-4.1}$	$^{-1.3}_{-1.6}$	$^{+8.2}_{-6.8}$	$^{+2.5}_{-5.0}$	$^{+9.7}_{-7.7}$	$^{+5.9}_{-5.5}$	$^{+11}_{-16}$	$^{+9.9}_{-13}$
Mistag Rate	$^{+1.3}_{-2.9}$	$^{-7.5}_{+1.8}$	$^{+18}_{-8.9}$	$^{+4.3}_{-6.6}$	$^{-0.2}_{+2.6}$	$^{-2.0}_{+1.0}$	$^{+8.2}_{-8.7}$	$^{+2.5}_{-2.2}$	$^{+8.1}_{-3.4}$	$^{+1.3}_{-0.5}$
Jet Energy Scale	$^{+19}_{-16}$	$^{+7.5}_{-7.5}$	$^{+17}_{-15}$	$^{+7.1}_{-14}$	$^{+18}_{-17}$	$^{+7.0}_{-4.7}$	$^{+16}_{-16}$	$^{+6.7}_{-3.3}$	$^{+15}_{-15}$	$^{-2.7}_{-8.1}$
ISR+FSR+PDF	$^{+10}_{-1.2}$	$^{-0.0}_{+0.0}$	$^{+14}_{-1.0}$	$^{-0.2}_{+0.2}$	$^{+8.2}_{-6.5}$	$^{+0.0}_{-0.0}$	$^{+12}_{-5.1}$	$^{-2.1}_{+2.1}$	$^{+14}_{-2.0}$	$^{-1.9}_{+1.9}$

TABLE XXVIII: Systematic uncertainties on the signal and background contributions for CDF's $t\bar{t}H$ 2-tag and 3-tag $\not\!\!E_T$+jets channels. Systematic uncertainties are listed by name; see the original references for a detailed explanation of their meaning and on how they are derived. Systematic uncertainties for $t\bar{t}H$ shown in this table are obtained for $m_H = 120$ GeV/c^2. Uncertainties are relative, in percent, and are symmetric unless otherwise indicated.

CDF: $t\bar{t}H$ $\not\!\!E_T$+jets 2-tag channel relative uncertainties (%)

Contribution	non-$t\bar{t}$	$t\bar{t}$	$t\bar{t}H$
Luminosity ($\sigma_{\rm inel}(p\bar{p})$)	0	3.8	3.8
Luminosity Monitor	0	4.4	4.4
Jet Energy Scale	0	2	11
Trigger Efficiency	0	7	7
B-Tag Efficiency	0	7	7
ISR/FSR	0	2	2
PDF	0	2	2
$t\bar{t}$ Cross Section	0	10	0
$t\bar{t}b\bar{b}$ Cross Section	0	3	0
Signal Cross Section	0	0	10
Background Modeling	6	0	0
Background B-tagging	5	0	0

CDF: $t\bar{t}H$ $\not\!\!E_T$+jets 3-tag channel relative uncertainties (%)

Contribution	non-$t\bar{t}$	$t\bar{t}$	$t\bar{t}H$
Luminosity ($\sigma_{\rm inel}(p\bar{p})$)	0	3.8	3.8
Luminosity Monitor	0	4.4	4.4
Jet Energy Scale	0	3	13
Trigger Efficiency	0	7	7
B-Tag Efficiency	0	9	9
ISR/FSR	0	2	2
PDF	0	2	2
$t\bar{t}$ Cross Section	0	10	0
$t\bar{t}b\bar{b}$ Cross Section	0	5	0
Signal Cross Section	0	0	10
Background Modeling	6	0	0
Background B-tagging	10	0	0

TABLE XXIX: Systematic uncertainties on the signal and background contributions for CDF's $t\bar{t}H$ 2-tag and 3-tag all jets channels. Systematic uncertainties are listed by name; see the original references for a detailed explanation of their meaning and on how they are derived. Systematic uncertainties for $t\bar{t}H$ shown in this table are obtained for $m_H = 120$ GeV/c^2. Uncertainties are relative, in percent, and are symmetric unless otherwise indicated.

CDF: $t\bar{t}H$ all jets 2-tag channel relative uncertainties (%)

Contribution	non-$t\bar{t}$	$t\bar{t}$	$t\bar{t}H$
Luminosity ($\sigma_{\text{inel}}(p\bar{p})$)	0	3.8	3.8
Luminosity Monitor	0	4.4	4.4
Jet Energy Scale	0	11	20
Trigger Efficiency	0	7	7
B-Tag Efficiency	0	7	7
ISR/FSR	0	2	2
PDF	0	2	2
$t\bar{t}$ Cross Section	0	10	0
$t\bar{t}b\bar{b}$ Cross Section	0	3	0
Signal Cross Section	0	0	10
Background Modeling	9	0	0
Background B-tagging	5	0	0

CDF: $t\bar{t}H$ all jets 3-tag channel relative uncertainties (%)

Contribution	non-$t\bar{t}$	$t\bar{t}$	$t\bar{t}H$
Luminosity ($\sigma_{\text{inel}}(p\bar{p})$)	0	3.8	3.8
Luminosity Monitor	0	4.4	4.4
Jet Energy Scale	0	13	22
Trigger Efficiency	0	7	7
B-Tag Efficiency	0	9	9
ISR/FSR	0	2	2
PDF	0	2	2
$t\bar{t}$ Cross Section	0	10	0
$t\bar{t}b\bar{b}$ Cross Section	0	6	0
Signal Cross Section	0	0	10
Background Modeling	9	0	0
Background B-tagging	10	0	0

TABLE XXX: Systematic uncertainties on the signal and background contributions for CDF's $H \to \tau^+\tau^-$ channels. Systematic uncertainties are listed by name; see the original references for a detailed explanation of their meaning and on how they are derived. Systematic uncertainties for the Higgs signal shown in these tables are obtained for $m_H = 120$ GeV/c^2. Uncertainties are relative, in percent, and are symmetric unless otherwise indicated. Shape uncertainties are labeled with an "S".

CDF: $H \to \tau^+\tau^-$ channel relative uncertainties (%)

Contribution	$Z/\gamma^* \to \tau\tau$	$Z/\gamma^* \to ee$	$Z/\gamma^* \to \mu\mu$	$t\bar{t}$	diboson	fakes from SS	W+jets	WH	ZH	VBF	$gg \to H$
PDF Uncertainty	1	1	1	1	1	-	-	1.2	0.9	2.2	4.9
ISR 1 JET	-	-	-	-	-	-	-	-6.9	-2.9	-1.8	11.8
ISR $\geq$ 2 JETS	-	-	-	-	-	-	-	-0.5	0.1	-1.9	18.1
FSR 1 JET	-	-	-	-	-	-	-	4.3	0.7	1.1	-3.4
FSR $\geq$ 2 JETS	-	-	-	-	-	-	-	-0.9	-0.5	-1.0	-5.0
JES (S) 1 JET	7.9	7.6	3.9	-8.4	6.3	-	-	-4.8	-5.3	-3.7	5.1
JES (S) $\geq$ 2 JETS	14.0	11.0	20.1	2.8	11.7	-	-	5.4	4.8	-5.2	13.2
Normalization 1 JET	2.2	2.2	2.2	10	6	10	25	5	5	10	23.5
Normalization $\geq$2 JETS	2.2	2.2	2.2	10	6	10	30	5	5	10	67.5
MC Acceptance	2.3	2.3	2.3	-	-	-	-	-	-	-	-
ε_{trig} (e/μ leg)	-	0.3	1.0	-	-	-	-	-	-	-	-
ε_{trig} (τ leg)	-	3.0	3.0	-	-	-	-	-	-	-	-
$\varepsilon_{ID}lep$	-	2.4	2.6	-	-	-	-	-	-	-	-
ε_{vtx}	-	0.5	0.5	-	-	-	-	-	-	-	-
e/$\mu \to \tau_h$ fake rate	-	7.4	15.5	-	-	-	-	-	-	-	-
Luminosity	-	5.9	5.9	-	-	-	-	-	-	-	-
tau ID scale factor:											
N_{obs}	1.8	-	-	1.8	1.8	-	-	1.8	1.8	1.8	1.8
N_{SSdata}	-3.7	-	-	-3.7	-3.7	-	-	-3.7	-3.7	-3.7	-3.7
N_{W+jets}	-1.6	-	-	-1.6	-1.6	-	-	-1.6	-1.6	-1.6	-1.6
Cross section (DY)	-2.1	-	-	-2.1	-2.1	-	-	-2.1	-2.1	-2.1	-2.1
MC Acceptance (DY)	-2.2	-	-	-2.2	-2.2	-	-	-2.2	-2.2	-2.2	-2.2
e/$\mu \to \tau_h$ fake rate	-0.1	-	-	-0.1	-0.1	-	-	-0.1	-0.1	-0.1	-0.1

TABLE XXXI: Systematic uncertainties on the signal and background contributions for CDF's $WH \to \ell\nu\tau^+\tau^-$ and $ZH \to \ell^+\ell^-\tau^+\tau^-$ channels. Systematic uncertainties are listed by name; see the original references for a detailed explanation of their meaning and on how they are derived. Systematic uncertainties for the Higgs signal shown in these tables are obtained for $m_H = 120$ GeV/c^2. Uncertainties are relative, in percent, and are symmetric unless otherwise indicated.

CDF: $WH \to \ell\nu\tau^+\tau^-$ and $ZH \to \ell^+\ell^-\tau^+\tau^-$ $\ell\ell\tau_h + X$ channel relative uncertainties (%)

Contribution	ZZ	WZ	WW	$DY(ee)$	$DY(\mu\mu)$	$DY(\tau\tau)$	$Z\gamma$	$t\bar{t}$	$W\gamma$	$W+jet$	WH	ZH	VBF	$gg \to H$
Luminosity	5.9	5.9	5.9	5.9	5.9	5.9	5.9	5.9	5.9	5.9	5.9	5.9	5.9	5.9
Cross Section	11.7	11.7	11.7	5.0	5.0	5.0	11.7	14.1	11.7	5.0	5.0	5.0	10.0	10.0
Z-vertex Cut Efficiency	0.5	0.5	0.5	0.5	0.5	0.5	0.5	0.5	0.5	0.5	0.5	0.5	0.5	0.5
Trigger Efficiency	1.1	1.1	1.0	1.0	1.0	1.1	1.1	1.0	0.8	1.0	1.2	1.2	1.2	1.1
Lepton ID Efficiency	2.4	2.3	2.4	2.4	2.4	2.4	2.4	2.4	2.3	2.4	2.4	2.4	2.4	2.4
Lepton Fake Rate	10.7	8.0	26.7	26.0	26.6	15.1	27.1	22.4	22.8	28.7	2.9	2.3	15.1	13.6
Jet Energy Scale	1.3	1.1	0.0	3.2	5.1	0.6	6.6	0.1	2.0	0.2	0.1	0.03	0.6	0.4
MC stat	3.7	2.9	7.6	1.5	1.7	2.2	4.1	3.1	20.0	3.1	1.5	1.4	3.8	9.4
PDF Model	-	-	-	-	-	-	-	-	-	-	1.2	0.9	2.2	4.9
ISR/FSR Uncertainties	-	-	-	-	-	-	-	-	-	-	1.3	2.1	0.6	0.2

CDF: $WH \to \ell\nu\tau^+\tau^-$ and $ZH \to \ell^+\ell^-\tau^+\tau^-$ $e\mu\tau_h + X$ channel relative uncertainties (%)

Contribution	ZZ	WZ	WW	$DY(ee)$	$DY(\mu\mu)$	$DY(\tau\tau)$	$Z\gamma$	$t\bar{t}$	$W\gamma$	$W+jet$	WH	ZH	VBF	$gg \to H$
Luminosity	5.9	5.9	5.9	5.9	5.9	5.9	5.9	5.9	5.9	5.9	5.9	5.9	5.9	5.9
Cross Section	11.7	11.7	11.7	5.0	5.0	5.0	11.7	14.1	11.7	5.0	5.0	5.0	10.0	10.0
Z-vertex Cut Efficiency	0.5	0.5	0.5	0.5	0.5	0.5	0.5	0.5	0.5	0.5	0.5	0.5	0.5	0.5
Trigger Efficiency	1.4	1.4	1.1	1.1	1.3	1.1	1.4	1.1	1.0	0.7	1.3	1.3	1.2	1.2
Lepton ID Efficiency	2.4	2.4	2.4	2.4	2.4	2.4	2.4	2.4	2.4	2.4	2.4	2.4	2.4	2.4
Lepton Fake Rate	9.0	6.5	26.6	20.8	31.4	25.2	39.4	27.8	19.3	41.9	1.6	2.5	28.5	29.2
Jet Energy Scale	0.0	0.3	2.2	0.0	0.8	1.5	0.5	0.8	0.0	0.0	0.2	0.1	1.7	0.0
MC stat	12.9	7.2	20.9	57.7	12.6	7.7	10.2	12.4	35.4	25.8	2.1	3.9	13.0	44.7
PDF Model	-	-	-	-	-	-	-	-	-	-	1.2	0.9	2.2	4.9
ISR/FSR Uncertainties	-	-	-	-	-	-	-	-	-	-	0.6	0.2	0.1	0.0

CDF: $WH \to \ell\nu\tau^+\tau^-$ and $ZH \to \ell^+\ell^-\tau^+\tau^-$ $\ell\tau_h\tau_h + X$ channel relative uncertainties (%)

Contribution	ZZ	WZ	WW	$DY(ee)$	$DY(\mu\mu)$	$DY(\tau\tau)$	$Z\gamma$	$t\bar{t}$	$W\gamma$	$W+jet$	WH	ZH	VBF	$gg \to H$
Luminosity	5.9	5.9	5.9	5.9	5.9	5.9	5.9	5.9	5.9	5.9	5.9	5.9	5.9	5.9
Cross Section	11.7	11.7	11.7	5.0	5.0	5.0	11.7	14.1	11.7	5.0	5.0	5.0	10.0	10.0
Z-vertex Cut Efficiency	0.5	0.5	0.5	0.5	0.5	0.5	0.5	0.5	0.5	0.5	0.5	0.5	0.5	0.5
Trigger Efficiency	1.0	1.1	0.9	1.0	1.1	1.1	1.1	1.0	0.7	0.9	1.1	1.1	1.1	1.1
Lepton ID Efficiency	3.3	3.3	3.3	3.3	3.3	3.3	3.3	3.3	3.3	3.3	3.3	3.3	3.3	3.3
Lepton Fake Rate	10.4	6.8	38.1	43.3	39.9	24.8	32.8	34.2	28.8	34.8	3.1	5.9	28.1	26.3
Jet Energy Scale	5.5	0.0	0.0	3.3	1.6	1.2	1.6	0.0	0.0	1.1	0.1	0.6	1.8	1.7
MC stat	12.5	8.1	16.9	18.3	12.5	4.9	12.6	14.7	70.7	8.7	2.0	3.3	9.4	18.3
PDF Model	-	-	-	-	-	-	-	-	-	-	1.2	0.9	2.2	4.9
ISR/FSR Uncertainties	-	-	-	-	-	-	-	-	-	-	1.2	0.5	0.4	0.04

TABLE XXXII: Systematic uncertainties on the signal and background contributions for CDF's $WH + ZH \rightarrow jjbb$ and $VBF \rightarrow jjbb$ channels. Systematic uncertainties are listed by name; see the original references for a detailed explanation of their meaning and on how they are derived. Uncertainties with provided shape systematics are labeled with "s". Systematic uncertainties for H shown in this table are obtained for $m_H = 115$ GeV/c^2. Uncertainties are relative, in percent, and are symmetric unless otherwise indicated. The cross section uncertainties are uncorrelated with each other (except for single top and $t\bar{t}$, which are treated as correlated). The QCD uncertainty is also uncorrelated with other channels' QCD rate uncertainties.

CDF: $WH + ZH \rightarrow jjbb$ and $VBF \rightarrow jjbb$ channel relative uncertainties (%)

Contribution	$t\bar{t}$	diboson	W/Z+Jets	VH	VBF
Jet Energy Correction				7 s	7 s
PDF Modeling				2	2
SecVtx+SecVtx	7.6	7.6	7.6	7.6	7.6
SecVtx+JetProb	9.7	9.7	9.7	9.7	9.7
Luminosity	6	6	6	6	6
ISR/FSR modeling				2 s	3 s
Jet Moment				s	s
Trigger	4	4	4	4	4
QCD Interpolation				s	s
QCD MJJ Tuning				s	s
QCD Jet Moment Tuning				s	s
cross section	10	6	50		

TABLE XXXIII: Systematic uncertainties on the signal contributions for CDF's $H \rightarrow \gamma\gamma$ channels. Systematic uncertainties are listed by name; see the original references for a detailed explanation of their meaning and on how they are derived. Uncertainties are relative, in percent, and are symmetric unless otherwise indicated.

CDF: $H \rightarrow \gamma\gamma$ channel relative uncertainties (%)

Channel	CC	CP	CC Conv	PC Conv
Signal Uncertainties :				
Luminosity	6	6	6	6
$\sigma_{ggH}/\sigma_{VH}/\sigma_{VBF}$	14/7/5	14/7/5	14/7/5	14/7/5
PDF	2	2	2	2
ISR	3	4	2	5
FSR	3	4	2	5
Energy Scale	0.2	0.8	0.1	0.8
Trigger Efficiency	–	–	0.1	0.4
z Vertex	0.2	0.2	0.2	0.2
Conversion ID	–	–	7	7
Detector Material	0.4	3.0	0.2	3.0
Photon/Electron ID	1.0	2.8	1.0	2.6
Run Dependence	3.0	2.5	1.5	2.0
Data/MC Fits	0.4	0.8	1.5	2.0
Background Uncertainties :				
Fit Function	3.5	1.1	7.5	3.5

TABLE XXXIV: Systematic uncertainties on the signal and background contributions for D0's $H \to \gamma\gamma$ channel. Systematic uncertainties for the Higgs signal shown in this table are obtained for $m_H = 125$ GeV/c^2. Systematic uncertainties are listed by name; see the original references for a detailed explanation of their meaning and on how they are derived. Uncertainties are relative, in percent, and are symmetric unless otherwise indicated.

D0: $H \to \gamma\gamma$ channel relative uncertainties (%)

Contribution	Background	Signal
Luminosity	6	6
Acceptance	–	2
electron ID efficiency	2	–
electron track-match inefficiency	10	–
Photon ID efficiency	3	3
Photon energy scale	2	1
Cross Section	4	10
Background subtraction	15	-